

**ORNL/MD/LTR-236**

**MOX Average Power Test 40 GWd/MT  
PIE: Quick Look**

**R.N. Morris  
C.A. Baldwin  
N.H. Packan**

**November 2002**

**Fissile Materials Disposition Program**

**Notice**

**This report was prepared as an account of work sponsored by an agency of the United States Government. Neither the United States Government nor any agency thereof, or any of their employees, makes any warranty, expressed or implied, or assumes any legal liability or responsibility for any third party's use or the results of such use, of any information, apparatus, product or process disclosed in this report, or represents that its use by such third party would not infringe privately owned rights.**

### Revision History

<b>Revision number</b>	<b>Date Issued</b>	<b>Reason for revision</b>
0	November 2002	First Issue

## OAK RIDGE NATIONAL LABORATORY

MANAGED BY LOCKHEED MARTIN ENERGY RESEARCH CORPORATION  
FOR THE U.S. DEPARTMENT OF ENERGY

BLDG. 3525, M/S 6295, ROOM 106  
POST OFFICE BOX 2008  
OAK RIDGE, TENNESSEE 37831-6295  
TELEPHONE: 423-241-4237  
FACSIMILE: 423-576-7862

November 2002

Distribution

### **MOX Average Power Test 40 GWd/MT PIE: Quick Look**

The enclosed document details the MOX Average Power Test initial PIE that was performed on the 40 GWd/MT-withdrawal Capsules 4 and 13 under the guidance of the DOE-sponsored Fissile Materials Disposition Program (FMDP). This work was carried out at the Irradiated Fuels Examination Laboratory by the staff of the Metals and Ceramics Division of the Oak Ridge National Laboratory during the period from April 2002 through November 2002. A final report of the entire PIE for these capsules is scheduled for issue in June 2003.

This is a Level-2 document as defined in the Fissile Materials Disposition Program Light-Water Reactor Mixed-Oxide Fuel Irradiation Test Project Plan, ORNL/MD/LTR-78, Rev 2.

Sincerely,

Robert N. Morris  
Fissile Materials Disposition Program

Enclosure

Distribution: See Section 7 of enclosure

**MOX Average Power Test 40 GWd/MT PIE:  
Quick Look**

**R.N. Morris  
C.A. Baldwin  
N.H. Packan**

**November 2002**

Oak Ridge National Laboratory

## TABLE OF CONTENTS

<b>LIST OF FIGURES .....</b>	<b>vi</b>
<b>LIST OF TABLES .....</b>	<b>viii</b>
<b>ACRONYMS .....</b>	<b>ix</b>
<b>ABSTRACT.....</b>	<b>x</b>
<b>1. INTRODUCTION.....</b>	<b>1</b>
<b>2. IRRADIATION HISTORY AND CARTS PREDICTIONS FOR CAPSULES 4 AND 13 .....</b>	<b>2</b>
2.1 Irradiation History for Phase I .....	2
2.2 Irradiation History for Phase II.....	3
2.3 Irradiation History for Phase III Part 1 .....	4
2.4 Irradiation History for Phase IV Part 1 .....	4
2.5 Calculation Scope .....	5
2.6 CARTS Results for Capsule Conditions During the Irradiation.....	7
2.6.1 Results for Capsule 4 .....	7
2.6.1.1 The Halden Threshold.....	8
2.6.1.2 Effect of Fission Gas Release on Gap Conductance.....	10
2.6.1.3 Effect of Fission Gas Release on Fuel Radial Temperature Profile .....	10
2.6.2 Results for Capsule 13 .....	13
2.6.2.1 Halden Threshold for Capsule 13 .....	15
2.6.2.2 Effect of Fission Gas Release on Gap Conductance.....	15
2.7 In-Reactor Conditions at the End of Phase IV Part 1 .....	15
2.8 Predicted Conditions for the Capsules in the Hot Cell .....	16
2.9 Potential for Increased Gas Release Fraction .....	19
2.10 Summary and Conclusions from the CARTS Predictions.....	20
<b>3. “QUICK LOOK” PRELIMINARY PIE .....</b>	<b>22</b>
3.1 Capsule Photo Visual Inspection .....	22
3.2 Capsule Temperature Measurements.....	26
3.3 Capsule Dimensional Inspection.....	26
3.4 Capsule Gamma Scans.....	28
3.4.1 Capsule 4 Gamma Scan .....	28
3.4.2 Capsule 13 Gamma Scan .....	34
3.4.3 Gamma Scanner Data Collection Orientation.....	39
3.5 Fission Gas Measurements .....	39
3.6 Fuel Pin Photo Visual Inspections .....	42
3.7 Fuel Pin Dimensional Inspections .....	44
3.7.1 Fuel Pin Volume Measurement .....	45
<b>4.0 CONCLUSIONS FROM QUICK LOOK PIE.....</b>	<b>50</b>
<b>5.0 ACKNOWLEDGMENTS .....</b>	<b>51</b>
<b>6.0 REFERENCES.....</b>	<b>52</b>
<b>7.0 DISTRIBUTION .....</b>	<b>54</b>

## LIST OF FIGURES

Fig. 2.1. CARTS predictions for Capsule 4 with representation of outward clad creep and best-estimate fission gas release fractions. Individual traces show results for maximum, mean, and minimum initial pellet-clad and clad-capsule gap widths.	9
Fig. 2.2. Comparison of CARTS predictions for Capsule 4 (mean as-built dimensions) showing effects of upper-limit versus best-estimate fission gas release fractions.....	11
Fig. 2.3. Effect of upper-limit versus best-estimate fission gas release fractions on pellet radial temperature profile for Capsule 4 (mean as-built dimensions) at the end of irradiation. ....	12
Fig. 2.4. CARTS predictions for Capsule 13 with representation of outward clad creep and best-estimate fission gas release fractions. Individual traces show results for maximum, mean, and minimum initial pellet-clad and clad-capsule gap widths. ....	14
Fig. 2.5. Comparison of CARTS predictions for Capsule 13 (mean as-built dimensions) showing effects of upper-limit versus best-estimate fission gas release fractions.....	17
Figure 3.1. Side view of Capsule 4. Note the discoloration on the right 2/3 <sup>rd</sup> of the capsule. ...	24
Figure 3.2. Top view of Capsule 4.....	24
Figure 3.3. Bottom view of Capsule 4. ....	24
Figure 3.4. Side view of Capsule 13. The discoloration is similar to that on Capsule 4. ....	25
Figure 3.5. Top view of Capsule 13.....	25
Figure 3.6. Bottom view of Capsule 13. ....	25
Figure 3.7. Free air temperature measurement on Capsule 4. ....	27
Figure 3.8. Schematic of diameter measurement.....	27
Figure 3.9. Capsule 4 mid energy gamma raster scan. ....	29
Figure 3.10. Capsule 4 high-energy gamma raster scan. ....	31
Figure 3.11. Capsule 4 mid energy gamma line scan. ....	32
Figure 3.12. Capsule 4 high-energy gamma line scan. ....	33
Figure 3.13. Capsule 13 mid energy gamma raster scan. ....	35
Figure 3.14. Capsule 13 high-energy gamma raster scan. ....	36
Figure 3.15. Capsule 13 mid energy gamma line scan. ....	37
Figure 3.16. Capsule 13 high-energy gamma line scan. ....	38
Figure 3.17 Orientation of the capsule and the gamma scanner collimator/detector.....	39
Figure 3.18. Cross sectional view of the Fission Gas Pressure Measuring Apparatus. [Drill Schematic 3.wpg] .....	40
Figure 3.19. Side view of Fuel Pin 7 (foreground). Shown in the background are the components of the capsule. ....	42
Figure 3.20. Top view of Fuel Pin 7. The puncture hole can be seen.....	42
Figure 3.21. Bottom view of Fuel Pin 7. The vertical mark on the pedestal is a nick made when sawing the capsule bottom off.....	43
Figure 3.22. Side view of Fuel Pin 16 (foreground). Shown in the background are the components of the capsule. The small cut off piece of the capsule was used as a spacer when resolving the broken drill problem. ....	43
Figure 3.23. Top view of Fuel Pin 16. A piece of the broken drill bit can be seen in the partially drilled hole.....	44

Figure 3.24. Bottom view of Fuel Pin 16.....	44
Figure 3.25. Graph of Fuel Pin 7 diametrical measurements. ....	47
Figure 3.26. Graph of Fuel Pin 16 diametrical measurements. Both pressurized and unpressurized measurements are shown. (The unpressurized measurement had three small handling scratches at approximately 1.8, 2, and 3”, which were removed from the graph for clarity) .....	48
Figure 3.27. Schematic of the Fuel Pin Volume Measuring Apparatus. ....	49

## LIST OF TABLES

Table 2.1. Capsule heating rates for Phase I.....	3
Table 2.2. Capsule heating rates for Phase II.....	3
Table 2.3. Capsule heating rates for Phase III Part 1.....	4
Table 2.4. Capsule heating rates for Phase IV Part 1.....	5
Table 2.5. Results of CARTS calculations for Capsules 4 and 13 just prior to end of Phase IV Part 1.....	16
Table 2.6. CARTS predictions for Capsules 4 and 13 under hot cell conditions (mid-July 2002) .....	18
Table 2.7. Gas contents within Capsule-4 and -13 fuel as predicted by MOCUP calculations...	19
Table 3.1. Quick Look Metrology .....	22
Table 3.2. Capsule and Fuel Pin Numbers.....	23
Table 3.3. Capsule 4 and 13 Temperature Measurements .....	26
Table 3.4. Capsule Measurements .....	28
Table 3.5. Fission Gas Measurements .....	41
Table 3.6. Fuel Pin 7 and 16 Length and Weight .....	45
Table 4.1 Fission Gas Release Results .....	50

## ACRONYMS

APT	Average Power Test
ATR	Advanced Test Reactor
BOL	Beginning of Life
CARTS	Capsule Assembly Response-Thermal Swelling (Code)
EFPD	Effective Full Power Days
FGPMA	Fission Gas Pressure Measuring Apparatus
FMDP	Fissile Materials Disposition Program
GWd/MT	Giga-Watt Days per Metric Ton
INEEL	Idaho National Engineering and Environmental Laboratory
LANL	Los Alamos National Laboratory
LHGR	Linear Heat Generation Rate
LWR	Light Water Reactor
MCNP	Monte Carlo Neutron Photon (Code)
Mils	0.001 inches
MOX	Mixed Oxide
NRC	Nuclear Regulatory Commission
ORNL	Oak Ridge National Laboratory
PIE	Post Irradiation Examination
PPB	Parts Per Billion
PPM	Parts Per Million
PWR	Pressurized Water Reactor
RG	Reactor Grade
RMAL	Radioactive Materials Analysis Laboratory
TD	Theoretical Density
TIGR	Thermally Induced Gallium Removal
WG	Weapons Grade

## ABSTRACT

This report summarizes the early results of the post irradiation examination of the 40 GWd/MT MOX Average Power Test Capsules (numbers 4 and 13). The purpose of this preliminary examination is to document and monitor the progress of the MOX Average Power Test Irradiation. The capsules and their fuel pins were found to be in excellent condition. The gas pressure measurements and fission gas releases were higher than expected (based on past PIEs performed for similar fuel at lower burnups), but still lower than the European experience for similar irradiation histories. The fission gas release fractions based on  $^{85}\text{Kr}$  activity measurements were in the range of 6.2 to 6.8%. Preliminary fuel stack gamma scan measurements and fuel pin diameter measurements indicate that the fuel is behaving as expected for the irradiation conditions experienced.

# 1. INTRODUCTION

This is the seventh report in a series of reports detailing the post irradiation examination (PIE) of the Fissile Materials Disposition Program (FMDP) Average Power MOX irradiation tests [Reference 1]. These tests are investigating the use of weapons grade (WG) plutonium in mixed oxide (MOX) fuel for light-water reactors (LWR) to demonstrate that the substitution of weapons-derived plutonium for the reactor grade (RG) plutonium used in commercial MOX fuel does not negatively affect the performance of the fuel system and, thus, the commercial database is applicable. To meet this end, this test program was created to fabricate, assemble, and irradiate small test capsules containing weapons-derived MOX at expected fuel average power conditions, 6-10 kW/ft.

Simple, uninstrumented, drop-in capsules with local flux monitor wires were fabricated and placed in the Advanced Test Reactor (ATR) at Idaho National Engineering and Environmental Laboratory (INEEL). The average power test program comprises 13 capsules, 7 of which contain MOX fuel prepared without a gallium removal step, and 6 of which contain fuel in which the PuO<sub>2</sub> was treated with a special gallium removal step. The target irradiation goal is 50 GWd/MT for three capsules, while other capsules have been removed at 8, 21, 30, and 40 GWd/MT for the purpose of monitoring the irradiation, and two capsules have been designated as unirradiated archives. The topic of this report is the early examination of the two capsules that have been withdrawn after irradiation to 40 GWd/MT; six previous reports have dealt with the PIEs at 8 GWd/MT, 21 GWd/MT, and 30 GWd/MT [References 2-7].

As in the previous PIEs, the examination of the MOX capsules removed at 40 GWd/MT will be conducted in two steps. The first step is a "quick look", whose purpose is to determine the gross physical state of the capsule, cladding, and fuel. This first step is the topic of this report. The major goal of the quick look is to provide feedback to the irradiation group on issues that may impact the continued and safe operation of the capsules remaining in the ATR. This step also evaluates the usefulness of the current test apparatus and techniques for their role in the MOX irradiation task.

The second PIE step is a more detailed examination of the capsules for the purpose of collecting general cladding and fuel performance data for the FMDP program. The results of the second step PIE will be discussed in a final report for the 40 GWd/MT PIE scheduled for issue in June 2003.

The general PIE plan is detailed in Reference 8. However, modifications to this plan may be implemented by approved procedure changes, especially in the areas of gallium analysis and clad testing, so the current FMDP PIE program manager should be consulted for details concerning the status of current PIE tasks.

## **2. IRRADIATION HISTORY AND CARTS PREDICTIONS FOR CAPSULES 4 AND 13**

**S.A. Hodge**

**L.J. Ott**

This Chapter reports the results of calculations performed by Nuclear Science and Technology Division staff in advance of the postirradiation examination (PIE) for the capsules withdrawn at 40 GWd/MT. These are Capsules 4 and 13, which occupied various symmetric test assembly positions during irradiation Phases I, II, III Part 1, and IV Part 1, thereby accumulating a total of 904 EFPDs. The pellet, fuel pin, and capsule behaviors across an average pellet midplane during the as-run irradiations are predicted by application of the Capsule Assembly Response-Thermal Swelling (CARTS) code. In essence, CARTS determines the quasi-steady state coupled thermal/mechanical solutions at each point in a series of stepwise advances in integrated internal energy release. Separate calculations were carried out for Capsules 4 and 13.

For each irradiation cycle, the CARTS input comprises the integrated energy release per unit heavy metal and the associated average linear heat generation rate (LHGR) during the cycle. The integrated energy release is calculated for nominal fuel stack dimensions and fuel mass by the MCNP code and derives from all sources, including fission product decay and gamma heating by the ATR core. The CARTS input is then obtained for the individual capsules by adjusting for the actual fuel mass and pellet stack height.

The following Sections describe the irradiation phases and the associated CARTS input for Capsules 4 and 13. Capsule 4 carried Fuel Pin 7 with a pellet stack height of 5.82 inch and a heavy metal mass of 71.754 gm. Capsule 13 carried Fuel Pin 16 with TIGR-treated fuel, a stack height of 5.79 inch and a heavy metal mass of 72.142 gm.

### **2.1 Irradiation History for Phase I**

The 155 effective full power days (EFPDs) leading up to the withdrawal of Capsules 1 and 8 for the early PIE collectively constitute irradiation Phase I. This phase, which extended from February 5 until September 13, 1998, comprises Advanced Test Reactor (ATR) Cycles 115C through 117B. The Inconel shield basket assembly (Model 1) was employed throughout. Capsules 4 and 13 occupied, respectively, the upper and lower back positions within the test assembly.

The accumulated burnups and associated average linear heat generation rates (LHGRs) for Capsules 4 and 13 during the individual irradiation cycles of Phase I are listed in Table 2.1. These values are lower than those experienced by the capsules withdrawn for previous PIEs because Capsules 4 and 13 occupied positions of lower neutron flux during the Phase-I irradiation.

**Table 2.1. Capsule heating rates for Phase I**

Cycle	EFPDs	Capsule 4			Capsule 13		
		MWd	Average LHGR KW/ft	End-cycle burnup GWd/MT	MWd	Average LHGR KW/ft	End-cycle burnup GWd/MT
115C	48.4	0.1435	6.118	2.04	0.1457	6.240	2.19
116A	12.8	0.0337	5.436	2.52	0.0346	5.607	2.70
116B	22.2	0.0653	6.069	3.45	0.0664	6.196	3.70
117A	14.1	0.0380	5.565	3.99	0.0382	5.620	4.27
117B	57.4	0.1593	5.726	6.25	0.1558	5.626	6.61

There were two brief unplanned ATR shutdowns during Cycle 115C and another during Cycle 116A. Thus, the test capsules were thermally cycled eight times during the five ATR operating cycles of the Phase-I irradiation. Capsules 1 and 8 were withdrawn at the completion of Phase I and shipped to ORNL for PIE.

## 2.2 Irradiation History for Phase II

The Phase-II irradiation began on November 9, 1998, and continued for 228 EFPDs, ending September 12, 1999. This period comprised ATR Cycles 118A through 120A, for which the Model 2 aluminum-shield basket was employed throughout. The test assembly was loaded with seven irradiated capsules carried over from Phase I, plus two new fresh fuel capsules (6 and 12) to replace Capsules 1 and 8. Capsules 4 and 13 occupied the front middle positions during Phase II, with accumulated burnup and average cycle LHGRs as listed in Table 2.2.

**Table 2.2. Capsule heating rates for Phase II**

Cycle	EFPDs	Capsule 4			Capsule 13		
		MWd	Average LHGR KW/ft	End-cycle burnup GWd/MT	MWd	Average LHGR KW/ft	End-cycle burnup GWd/MT
118A(1)	27.4	0.1414	10.644	8.13	0.1421	10.750	8.17
118A(2)	21.0	0.1069	10.504	9.63	0.1082	10.680	9.69
118B	36.4	0.1772	10.046	12.11	0.1811	10.310	12.22
119A(1)	19.2	0.0619	6.654	12.97	0.0631	6.806	13.10
119A(2)	2.5	0.0105	8.646	13.12	0.0107	8.851	13.26
119A(3)	22.9	0.0984	8.864	14.50	0.1001	9.062	14.66
119B	42.1	0.1787	8.756	17.00	0.1782	8.772	17.16
120A	56.2	0.2174	7.982	20.04	0.2179	8.035	20.21

These LHGRs of greater than 10 kW/ft for Capsules 4 and 13 are the highest experienced by any capsule during this test irradiation.

With two brief unplanned shutdowns during Cycle 118B and one during Cycle 120A, the test capsules were thermally cycled 11 times during the eight operating cycles of Phase II. Capsules 2 and 9 were withdrawn at the end of Phase II and shipped to ORNL for PIE.

### 2.3 Irradiation History for Phase III Part 1

The Phase-III irradiation began on October 9, 1999, with ATR Cycle 120C. Part 1 continued through Cycle 122C, which ended July 23, 2000. The Model-2 aluminum-shield basket assembly was employed throughout. The test assembly was loaded with seven capsules carried over from Phase II. Capsules 4 and 13 occupied the front bottom positions during Phase III Part 1.

The test assembly loading pattern for Phase III Part 1 is illustrated by Figure 4 of the *ATR Capsule Assembly Loading and Operation Schedule*, ORNL/MD/LTR-91, Rev. 4. To complete the test assembly loading, the seven mixed-oxide (MOX) test capsules were augmented by two solid stainless steel dummy capsules, which occupied the two front middle positions within the test assembly.

The average LHGRs and accumulated burnups for Capsules 4 and 13 during the individual irradiation cycles of Phase III Part 1 are listed in Table 2.3.

**Table 2.3. Capsule heating rates for Phase III Part 1**

Cycle	EFPDs	Capsule 4			Capsule 13		
		MWd	Average LHGR KW/ft	End-cycle burnup GWd/MT	MWd	Average LHGR KW/ft	End-cycle burnup GWd/MT
120C	34.0	0.1091	6.619	21.59	0.1089	6.640	21.69
121A	14.0	0.0344	5.076	22.07	0.0361	5.340	22.19
121B(1)	19.5	0.0496	5.246	22.77	0.0534	5.674	22.94
121B(2)	26.8	0.0817	6.292	23.91	0.0786	6.081	24.04
121C	47.3	0.1277	5.571	25.70	0.1291	5.658	25.84
122A	40.9	0.1055	5.321	27.18	0.1053	5.337	27.31
122C	49.9	0.1306	5.400	29.01	0.1313	5.453	29.15

Total accumulated irradiation time was 232.4 EFPDs. With single unplanned shutdowns during Cycles 120C, 121B(2), 121C, and 122C, the test capsules were thermally cycled 11 times during the seven operating cycles of Phase III Part 1. Capsules 3 and 10 were withdrawn at the completion of Phase III Part 1 and sent to ORNL for PIE.

Phase III Part 2 comprised 113 EFPDs over three ATR cycles devoted to increasing the burnup of lag Capsules 5, 6, and 12. Capsules 4 and 13 rested in the ATR canal throughout the Part 2 irradiation.

### 2.4 Irradiation History for Phase IV Part 1

Irradiation for Phase IV Part 1 began with Cycle 124C on January 27, 2001, and continued through Cycle 127A, ending on March 9, 2002. The test assembly carried five MOX capsules and four stainless steel dummy capsules configured as shown in Figure 6 of the *ATR Capsule Assembly Loading and Operation Schedule*, ORNL/MD/LTR-91, Rev. 4. Capsules 4 and 13 occupied the front middle positions (the same as they had occupied during the Phase-II irradiation).

The CARTS code input for Capsules 4 and 13 during the individual cycles of Phase IV Part 1 represents the irradiation experience described in Table 2.4.

The Model-2 aluminum-shield basket assembly was employed throughout the 289 EFPDs of irradiation. Following Cycle 126A, the test assembly was shifted from the Northwest to the Southwest I-hole in the ATR reflector. The higher power in the ATR core Southwest Lobe (23 versus 17 MW) then produced the higher test capsule LHGRs as listed for the final two irradiation Cycles 126B and 127A.

With one unplanned shutdown-startup combination in both Cycles 125A(2) and 127A, the test capsules were thermally cycled 12 times during the ten operating cycles of Phase IV Part 1.

The cycle-by-cycle burnup accumulations for Capsules 4 and 13 are taken from the as-run Monte Carlo N-Particle (MCNP) code results obtained at Idaho National Engineering and Environmental Laboratory (INEEL) at the conclusion of each ATR operating cycle.

Uncertainties in these MCNP results are estimated to be  $\pm 7\%$  of the calculated value. An average LHGR is then derived for each cycle based on the cycle duration (EFPDs) and the actual test capsule fuel mass and stack length.

**Table 2.4. Capsule heating rates for Phase IV Part 1**

Cycle	EFPDs	Capsule 4			Capsule 13		
		MWd	Average LHGR KW/ft	End-cycle burnup GWd/MT	MWd	Average LHGR KW/ft	End-cycle burnup GWd/MT
124C(1)	5.0	0.0125	5.152	29.21	0.0124	5.143	29.35
124C(2)	3.4	0.0084	5.095	29.33	0.0084	5.101	29.46
124C(3)	18.7	0.0423	4.671	29.96	0.0428	4.741	30.09
124C(4)	13.0	0.0294	4.658	30.40	0.0288	4.589	30.53
125A(1)	31.9	0.0780	5.045	31.57	0.0776	5.039	31.68
125A(2)	22.1	0.0540	5.044	32.41	0.0538	5.040	32.51
125B	49.9	0.1091	4.510	34.11	0.1089	4.524	34.20
126A	39.7	0.0868	4.512	35.40	0.0873	4.557	35.49
126B	49.4	0.1543	6.443	37.67	0.1529	6.417	37.74
127A	56.0	0.1471	5.589	39.88	0.1493	5.700	39.96

Combining the Phase I, Phase II, Phase III Part 1, and Phase IV Part 1 experience, Capsules 4 and 13 were irradiated for 30 ATR operational cycles, accumulating 904.1 EFPDs (2.5 EFPY) and 42 thermal cycles. The final Fissions per Initial Metal Atom (FIMA) values are 4.15% for Capsule 4 and 4.16% for Capsule 13 (using conversion factor of 9.60 GWd/MT per FIMA percent). The overall EFPD-averaged LHGR for these capsules is 6.62 kW/ft, with a highest value of about 10.7 kW/ft at the beginning of Phase II. The integrated fast fluxes ( $E > 1.0$  MeV) are calculated (MCNP) as  $1.5E21$  (fuel),  $1.1E21$  (Zircaloy clad) and  $1.0E21$  (steel capsule).

## 2.5 Calculation Scope

CARTS calculations for Capsules 4 and 13 were run in advance of the PIE, each based upon the actual burnup accumulations and corresponding average LHGRs experienced during ATR

Cycles 115C through 122C (Phases I-III) and 124C through 127A (Phase IV). As described in the previous Sections, these capsules occupied a series of paired test assembly locations, symmetric with respect to the ATR core. Hence, their irradiation histories are similar.

The calculations predict the conditions at the pellet midplane as a function of increasing burnup, and do not include representation of pellet cracking, or end-effects such as hourglassing. Parameters varied are the initial pellet-to-clad and clad-to-capsule gap widths (minimum, mean, and maximum), and the extent of fission gas release (best-estimate and conservative). The fuel performance models correspond to those utilized within the FRAPCON code.

As noted in Section 2.2, Capsules 4 and 13 experienced their highest LHGRs during irradiation Phase II. Since the fuel centerline temperatures calculated for this period remain far below the MOX fuel melting temperature, it is clear that fuel melting is not of concern during these test irradiations. Rather, the potential (arising from the small initial pellet-clad gaps) for excessive fuel swelling against the fuel pin clad is the important concern. Accordingly, the CARTS analyses are primarily focused on the fuel swelling and densification models and the associated input parameters.

The FRAPCON-based CARTS calculations include the following features important to determination of the pellet temperature profile:

1. Fuel swelling at a constant rate of 0.77% per 10 GWd/MT burnup
2. MATPRO Correlation for Fuel Thermal Expansion
3. Fuel Thermal Conductivity Per Internal FRAPCON Correlation
4. Fuel Densification of 2.0%
5. Fuel Densification Completed by 10 GWd/MT
6. Parametric Variation of Fission Gas Release.

The cumulative fission gas release affects the gap conductance throughout the calculation and is controlled via a code input parameter specifying the percent released at 45 GWd/MT. The two values considered are defined from the European MOX experience as best estimate (4.2%) and conservative as determined by maximum LHGR (16.5% for Capsule 4 and 16.9% for Capsule 13).

The CARTS results provide a predicted range for the post-irradiation gaps as determined by the initial pellet-clad and clad-capsule gap widths. The FRAPCON fuel thermal conductivity correlation includes a degradation model that causes the fuel conductivity to decrease as burnup increases. This tends to increase the predicted pellet temperatures as irradiation proceeds, in turn causing a greater calculated thermal expansion. The considered densification of two percent complete by 10 GWd/MT burnup is selected to conform to the observations of the previous (30-GWd/MT) PIE.

These CARTS calculations also represent the progressive expansion of the clad as noted in the 30-GWd/MT PIE. This expansion is permanent, persisting after cooling has caused the pellet to shrink away from the clad inner surface. The extent of the outward clad deformation is small, about 0.15 mil per 10 GWd/MT burnup.

The calculations were advanced in steps of 0.01 GWd/MT, with data printout every 0.10 GWd/MT. Stepwise independence was confirmed by observing that results are virtually the same when one set was repeated with steps of 0.005 GWd/MT. The final advancement steps in each CARTS calculation represent conditions from the time that the capsules arrived at ORNL (April 2002) through the time (July 2002) that the fuel pins were expected to be opened for pellet inspection. For these three final calculation steps, the fuel pins are heated internally by decay power, while heat transfer from the outer capsule surface is by convection to the hot cell atmosphere.

## **2.6 CARTS Results for Capsule Conditions During the Irradiation**

Each capsule surrounds a fuel pin containing 15 MOX pellets. Each pellet has unique dimensions within the specified fabrication tolerances, so that a spectrum of initial pellet-to-clad gaps exists within each fuel pin. In the following discussions, results are reported for the minimum, mean, and maximum initial gap widths as defined by the measured fuel pin inner diameter and the tolerance range for pellet outer diameter.

Before proceeding to the conditions predicted for the capsule components in the hot cell, it is of interest to first consider the variations in pellet temperatures and diametral gaps as calculated for the period of irradiation, with particular attention to the conditions at the end of Phase IV Part 1, just prior to removal of the 40-GWd/MT capsules for PIE. It is important to recognize the inherent difference between the CARTS predictions reported here and the safety analyses previously performed for the burnup extension beyond 30 GWd/MT.

The current calculations are based on observations of pellet densification of 2.0 percent and outward clad creep, whereas the safety analyses assume no clad creep, and pellet densification limited to either zero or 0.5 percent. Without clad creep and with little fuel densification, clad contact is predicted at the pellet midplane, with the concomitant imposition of clad mechanical strain. This approach is appropriately conservative for the safety analyses. The more realistic analyses reported here predict that the pellet-clad midplane gap remains open, as discussed in the following subsections.

### **2.6.1 Results for Capsule 4**

Figure 2.1 illustrates the cycle-by-cycle LHGRs as calculated by the MCNP code for Capsule 4, with the corresponding CARTS predictions of pellet mean and centerline temperatures and variations in pellet-clad diametral gap. These parameters are plotted against the integrated internal energy release per unit heavy metal mass. The integrated energy release within the capsule is essentially equivalent to the fuel burnup, but includes power sources other than fission such as the small contribution of gamma heating by the ATR core. In the interest of avoiding unnecessary clutter, the LHGR trace does not include spikes to near zero to mark the between-cycle reactor outages.

Three traces are shown in each of the temperature and diametral gap plots, illustrating results as calculated for minimum, mean, and maximum initial pellet-to-clad gap widths. As indicated, the diametral gap is predicted to have remained open throughout the irradiation, with a closest

approach to closure (for the case of minimum initial gap) of about one-half mil near the end of Phase IV Part 1.

Unless otherwise stated, the following discussion will reflect the mean-value traces as shown in Figure 2.1. The ranges between the minimum and maximum traces on the temperature and diametral gap plots indicate the variations associated with pellet-specific differences in the initial pellet-clad gap width.

With pellet densification of 2.0 percent completed before burnup reaches 10.0 GWd/MT, the pellet diameter initially decreases and remains smaller than its initial value throughout Phase I. This pellet shrinkage combined with outward clad creep causes the predicted pellet-clad diametral gap to almost double (from 1.49 to 2.83 mils) during this period.

The highest LHGR experienced by Capsule 4 (10.64 kW/ft) was imposed at the beginning of Phase II. As indicated in Figure 2.1, the accompanying increase in pellet thermal expansion causes the pellet-clad gap to narrow to 1.60 mils. Reduced LHGRs during the subsequent cycles lower the pellet temperature with corresponding reductions in thermal expansion that tend to increase the pellet-clad gap. This trend is countered, however, by monotonically increasing fuel swelling as burnup accumulates. The gap width remains greater than its initial value until near the end of Phase III Part 1 (integrated energy release 27.2 GWd/MT).

As explained in Section 2.4, the increased LHGRs during the last two cycles of Phase IV Part 1 are due to the shift of the test assembly to the Southwest I-hole. The higher thermal expansion of the fuel during these cycles reduces the gap width to its smallest value during the irradiation.

As shown in Figure 2.1, the calculated pellet temperatures increase during periods while the LHGR remains constant during the Phase I and II irradiation cycles. This reflects the decreases in gap thermal conductance that accompany both an increasing gap width and the increasing inventories of low-conductivity fission gases. The opposite (temperature decrease with shrinking gap under constant LHGR) occurs during Phase IV Part 1.

The predicted temperatures are consistently higher for the calculation based on maximum initial pellet-clad gaps. This follows from the lower effective thermal conductance associated with wider gaps. Figure 2.1 shows that the highest predicted pellet centerline temperature (1576°C) occurs at the end of the second irradiation cycle of Phase II (9.5 GWd/MT). Since this is more than 1000°C below the melting temperature of the MOX fuel, there is no concern for the possibility of fuel melting.

No contact between fuel pin and capsule is predicted at any time during the irradiation.

### **2.6.1.1 The Halden Threshold**

The Halden empirical threshold for exceeding one percent gas release (described in Reference 9) has generally been found applicable to MOX as well as to the UO<sub>2</sub> fuel for which this criterion was originally developed. The Halden threshold is the burnup BU (GWd/MTHM) curve defined by the relation

## Capsule 4

ORNL 2002-0091C EFG

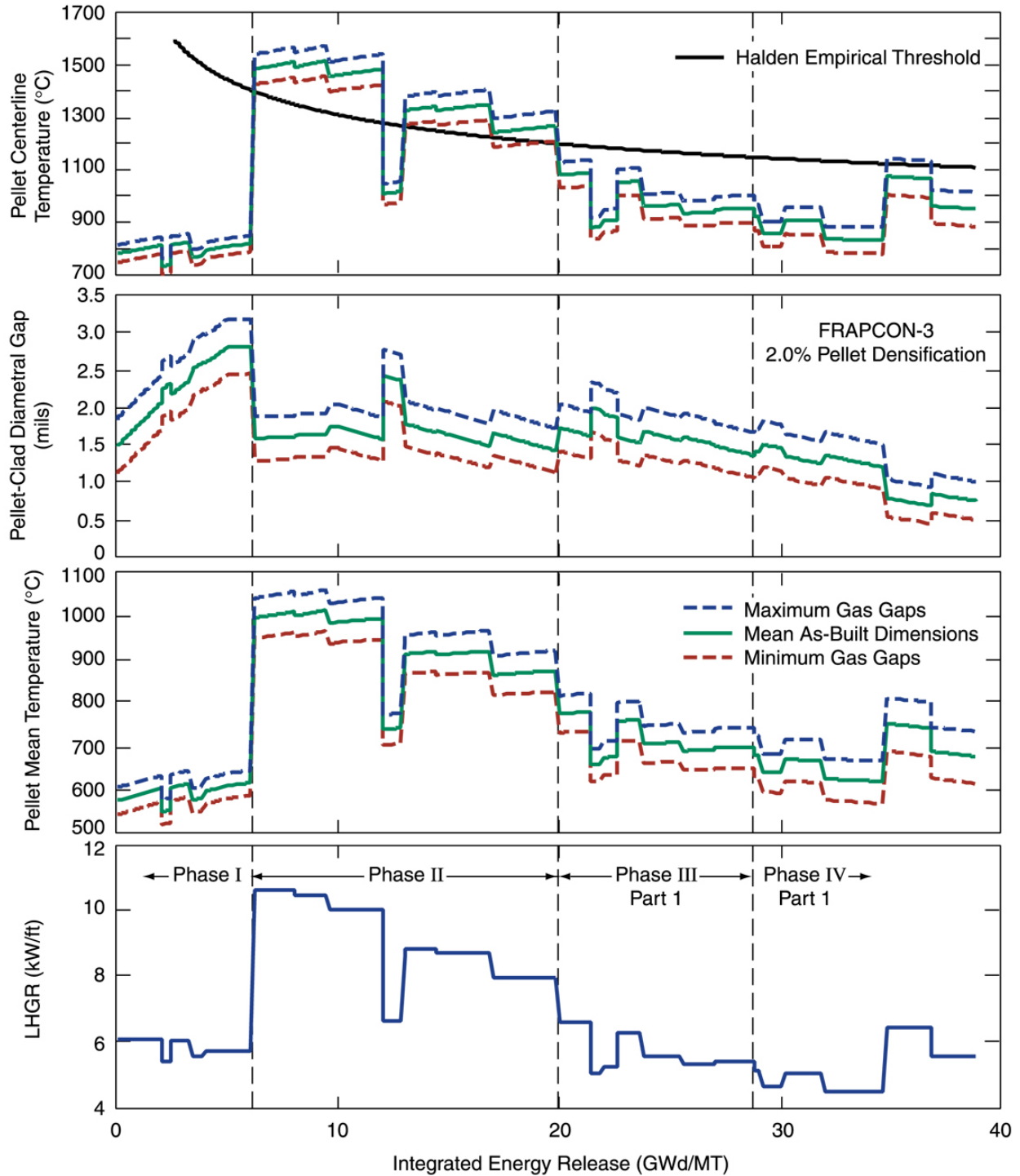


**Fig. 2.1. CARTS predictions for Capsule 4 with representation of outward clad creep and best-estimate fission gas release fractions. Individual traces show results for maximum, mean, and minimum initial pellet-clad and clad-capsule gap widths.**

$$BU = 0.00567e^{9800/T_c}$$

where  $T_c$  is the pellet centerline temperature. For example, for burnups of 10.65 GWd/MT (or greater), fission gas release in excess of one percent is expected if pellet centerline temperature exceeds 1300°C.

The upper plot in Figure 2.1 shows that the fuel centerline temperatures calculated for Capsule 4 exceed the Halden empirical threshold during almost all of Phase II, while the fuel burnup was advanced from 6.2 to 19.9 GWd/MT. The single exception is Cycle 119A(1) [12.1–12.9 GWd/MT]. The expected gas release fractions for Capsules 4 and 13 are discussed in Section 2.9.

### **2.6.1.2 Effect of Fission Gas Release on Gap Conductance**

The pellet-clad gap was initially filled with helium at atmospheric pressure. As irradiation proceeds, some fraction of the fission gases is released into this gap to mix with the helium. Since the thermal conductivities of krypton and xenon are much lower than that of helium, the effect is to significantly reduce the gap conductance.

The reduction in gap conductance serves to increase the fuel temperatures. Figure 2.2 illustrates the effect of fission gas on pellet temperatures by repeating the curves for mean initial gap width from Figure 2.1 (Best Estimate Fission Gas Release) and adding a second set of curves calculated with a higher (Upper Limit) fission gas release fraction. Here the best estimate corresponds to a 0.042 release at 45 GWd/MT while the upper limit corresponds to an assumed release of 0.165 at the same burnup. (See Section 3.3 of Reference 10 for the bases for these two values.)

The higher fuel temperatures associated with an increased gas release induce a greater thermal expansion of the pellet, which in turn reduces the pellet-clad gap width. This tends to reduce the fuel temperature and thereby serves as a stabilizing effect. Pellet swelling also reduces the gap width, which displaces much of the gas to the fuel pin gas plenum and narrows the difference between the best-estimate and upper-limit gas release curves at high burnups as shown in Figure 2.2.

### **2.6.1.3 Effect of Fission Gas Release on Fuel Radial Temperature Profile**

The radial temperature profile across the fuel as calculated for Capsule 4 just prior to the end of the irradiation is shown in Figure 2.3. Starting from the right side of the plot, straight lines represent the temperature increase across the capsule wall (average 98°C), the temperature jump at the clad-capsule gap, the temperature increase across the clad (average 232°C), and the temperature jump across the pellet-clad gap. When the calculation is repeated with the Upper Limit Fission Gas Release, the temperature increase across the pellet-clad gap is about 64°C greater, and the pellet centerline temperature is increased from 951°C to 1023°C.

# Capsule 4

ORNL 2002-0093C EFG

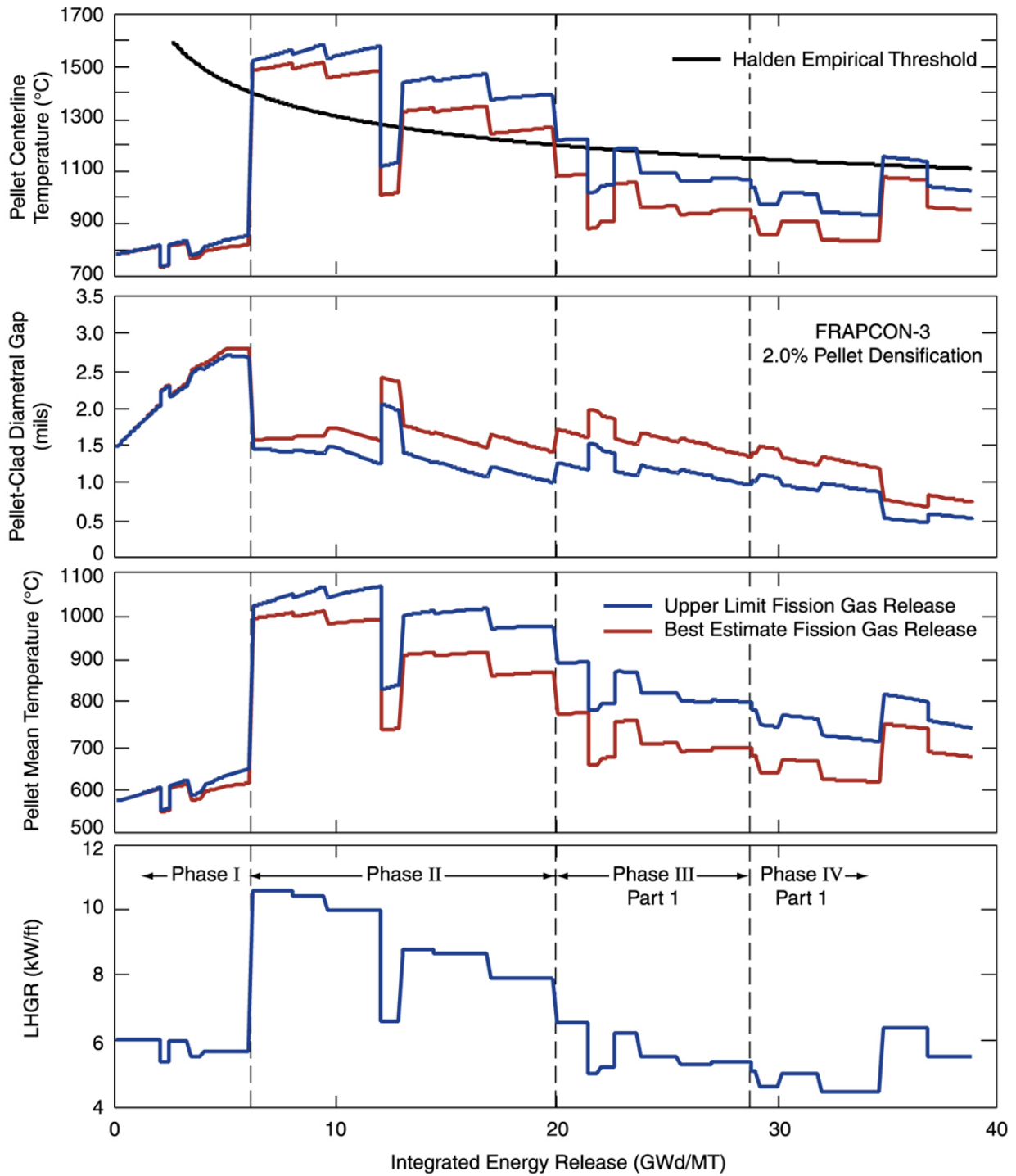


**Fig. 2.2. Comparison of CARTS predictions for Capsule 4 (mean as-built dimensions) showing effects of upper-limit versus best-estimate fission gas release fractions.**

# Capsule 4

ORNL 2002-0095C EFG

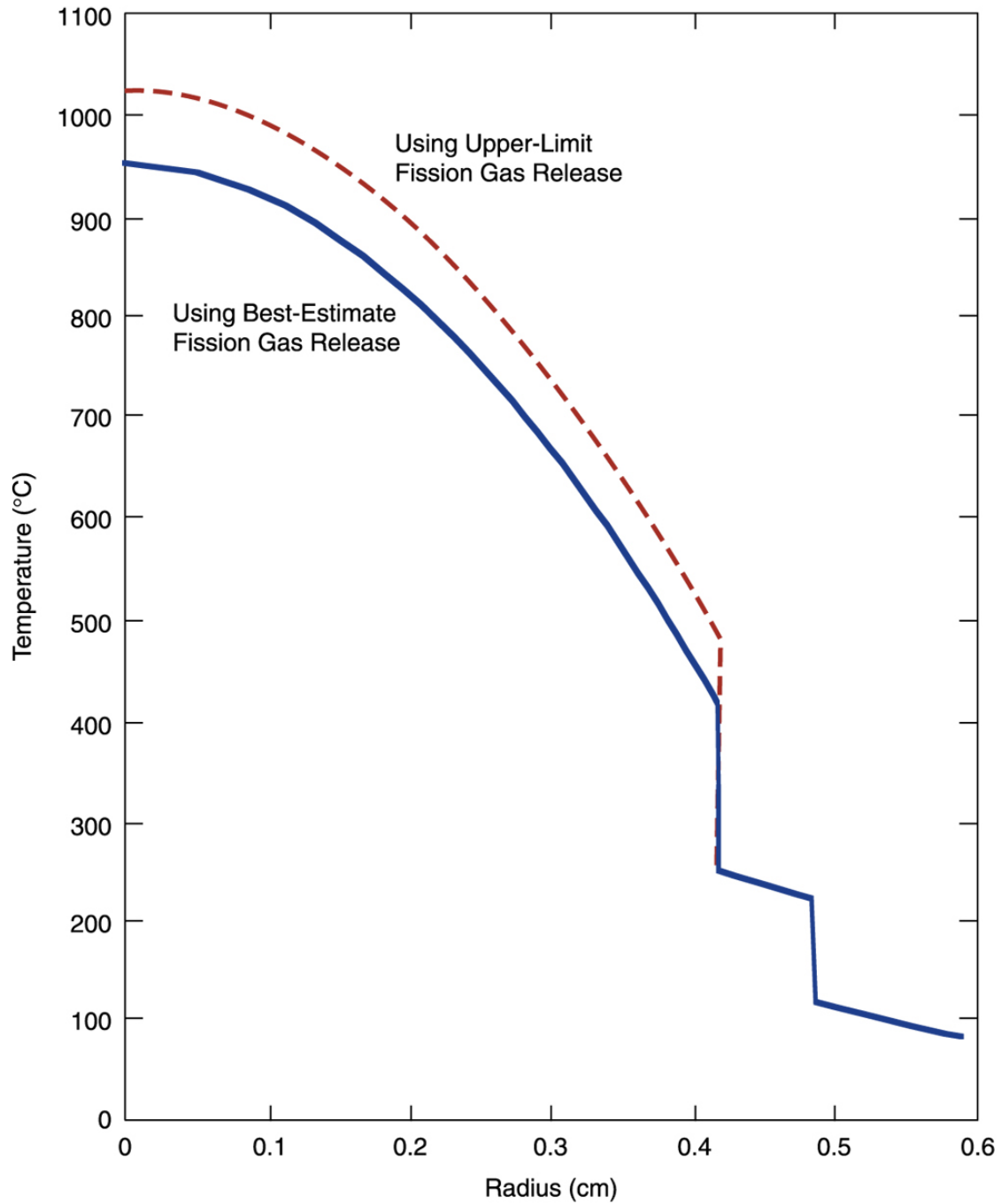


**Fig. 2.3. Effect of upper-limit versus best-estimate fission gas release fractions on pellet radial temperature profile for Capsule 4 (mean as-built dimensions) at the end of irradiation.**

## 2.6.2 Results for Capsule 13

The CARTS predictions of pellet mean and centerline temperatures and variations in pellet-clad diametral gap for Capsule 13 are shown in Figure 2.4. The three traces shown in each of the temperature and diametral gap plots illustrate results as calculated for minimum, mean, and maximum initial pellet-to-clad gap widths. Similar to the results for Capsule 4, the diametral gap is predicted to have remained open throughout the irradiation, with a closest approach to closure (for the case of minimum initial gap) of 0.50 mil near the end of Phase IV Part 1.

Previous PIE reports have presented irradiation histories as obtained from a single set of CARTS calculations based on the average LHGRs for the two capsules irradiated in symmetric positions. Capsules 4 and 13 were also irradiated in symmetric positions, but have been represented by independent CARTS calculations with separate input data sets based on the specific (measured) fuel pin and capsule dimensions and the individual LHGRs as calculated by the MCNP code at INEEL. Capsule 13 contains TIGR-treated fuel, and previous PIEs have suggested a difference in fission gas release between the TIGR and non-TIGR fuel. Accordingly, it was decided to maintain individual capsule irradiation histories for the 40- and 50-GWd/MT PIEs.

The differences in the irradiation histories for Capsules 4 and 13 are small. The Capsule 4 history is discussed in Section 2.6.1. The following discussions for Capsule 13 will reflect the mean-value traces as shown in Figure 2.4. The ranges between the minimum and maximum traces on the temperature and diametral gap plots indicate the variations associated with pellet-specific differences in the initial pellet-clad gap width.

With pellet densification of 2.0 percent completed before burnup reaches 10.0 GWd/MT, the pellet diameter initially decreases and remains smaller than its initial value throughout Phase I. This pellet shrinkage combined with outward clad creep causes the predicted pellet-clad diametral gap to almost double (from 1.46 to 2.86 mils) during this period.

The highest LHGR experienced by Capsule 13 (10.75 kW/ft) was imposed at the beginning of Phase II. As indicated in Figure 2.4, the accompanying increase in pellet thermal expansion causes the pellet-clad gap to narrow to 1.57 mils. Reduced LHGRs during the subsequent cycles lower the pellet temperature with corresponding reductions in thermal expansion that tend to increase the pellet-clad gap. This trend is countered, however, by monotonically increasing fuel swelling as burnup accumulates. The gap width remains greater than its initial value until near the end of Phase III Part 1 (integrated energy release 26.9 GWd/MT).

As explained in Section 2.4, the increased LHGRs during the last two cycles of Phase IV Part 1 are due to the shift of the test assembly to the Southwest I-hole. The higher thermal expansion of the fuel during these cycles reduces the gap width to its smallest value during the irradiation.

As shown in Figure 2.4, the calculated pellet temperatures increase during periods while the LHGR remains constant during the Phase I and II irradiation cycles. This reflects the decreases in gap thermal conductance that accompany both an increasing gap width and the increasing inventories of low-conductivity fission gases. The opposite (temperature decrease with shrinking gap under constant LHGR) occurs during Phase IV Part 1.

# Capsule 13

ORNL 2002-0092C EFG

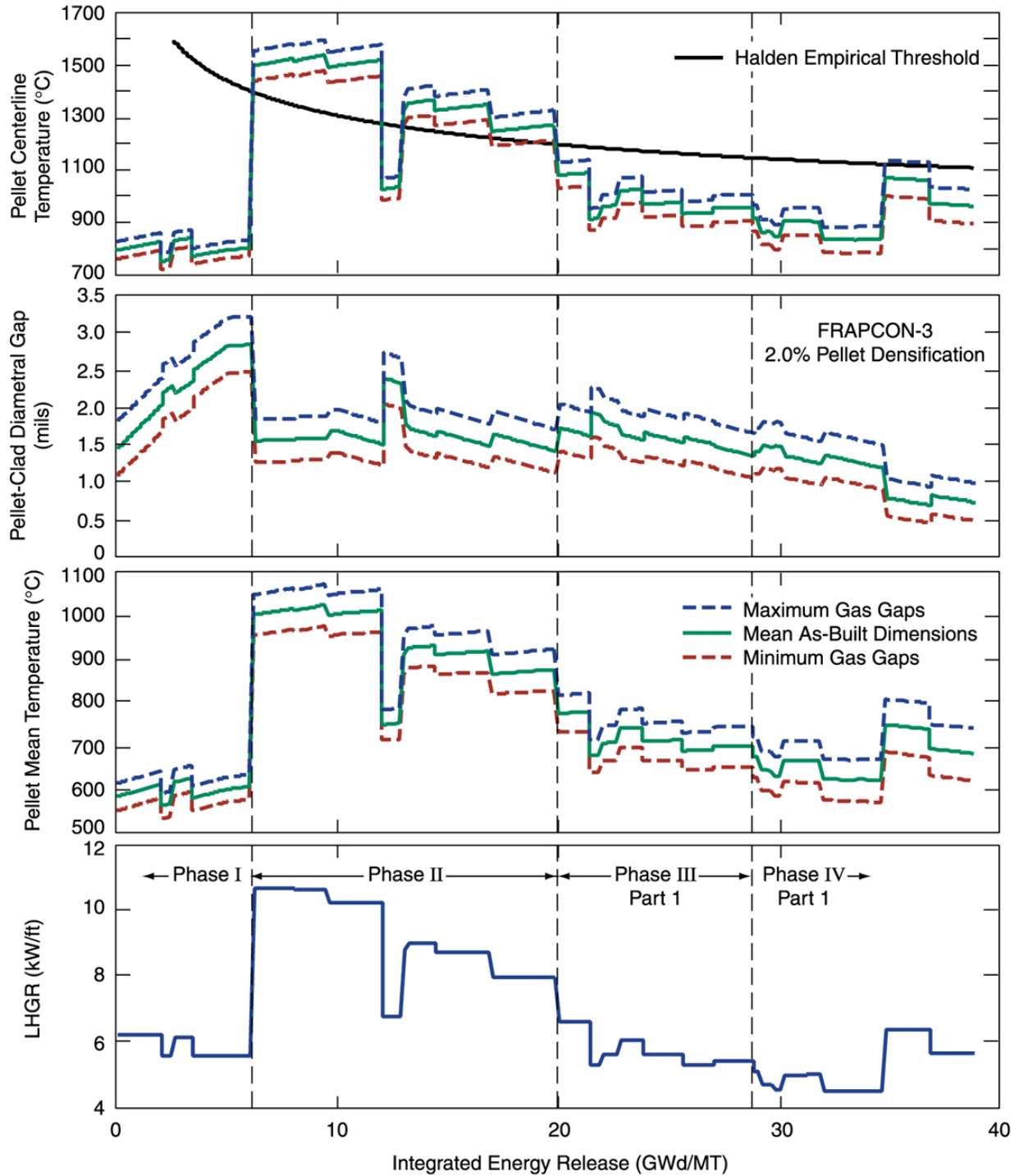


**Fig. 2.4. CARTS predictions for Capsule 13 with representation of outward clad creep and best-estimate fission gas release fractions. Individual traces show results for maximum, mean, and minimum initial pellet-clad and clad-capsule gap widths.**

The highest predicted pellet centerline temperature (1601°C) shown in Fig. 2.4 occurs for the case of maximum initial gaps at the end of the second irradiation cycle of Phase II (9.5 GWd/MT). Although this is slightly higher than the 1576°C predicted for Capsule 4, it remains more than 1000°C below the melting temperature of the MOX fuel with no concern for fuel melting.

No contact between fuel pin and capsule is predicted at any time during the irradiation.

### **2.6.2.1 Halden Threshold for Capsule 13**

The upper plot in Figure 2.4 shows that the fuel centerline temperatures calculated for Capsule 13 exceed the Halden empirical threshold during almost all of Phase II, while the fuel burnup was advanced from 6.2 to 19.9 GWd/MT. The single exception is Cycle 119A(1) [12.1–12.9 GWd/MT]. The extent to which the calculated centerline temperatures exceed the threshold is greatest for the pellets with maximum initial gap. The expected gas release fractions for Capsules 4 and 13 are discussed in Section 2.9.

### **2.6.2.2 Effect of Fission Gas Release on Gap Conductance**

The pellet-clad gap was initially filled with helium at atmospheric pressure. As irradiation proceeds, some fraction of the fission gases is released into this gap to mix with the helium. Since the thermal conductivity of krypton and xenon are much lower than that of helium, the effect is to significantly reduce the gap conductance.

The reduction in gap conductance serves to increase the fuel temperatures. Figure 2.5 illustrates the effect of fission gas on pellet temperatures by repeating the curves for mean initial gap width from Figure 2.4 (Best Estimate Fission Gas Release) and adding a second set of curves calculated with a higher (Upper Limit) fission gas release fraction. The best estimate corresponds to a 0.042 release at 45 GWd/MT while for Capsule 13 the upper limit corresponds to an assumed release of 0.169 at the same burnup. (See Section 3.3 of Reference 10 for the bases for these two values.)

The higher fuel temperatures associated with an increased gas release induce a greater thermal expansion of the pellet, which in turn reduces the pellet-clad gap width. This tends to reduce the fuel temperature and thereby serves as a stabilizing effect. Pellet swelling also reduces the gap width, which displaces much of the gas to the fuel pin gas plenum and narrows the difference between the two curves at high burnups as shown in Figure 2.5.

## **2.7 In-Reactor Conditions at the End of Phase IV Part 1**

Table 2.5 presents the results of the CARTS calculations for capsule conditions just prior to completion of the Phase IV Part 1 irradiation and withdrawal of Capsules 4 and 13 for PIE. Fuel burnup at this time was about 39.9 GWd/MT. As indicated in the last column of Table 2.5, none of these calculations predicts clad contact at the pellet midplane any time during the irradiation.

**Table 2.5. Results of CARTS calculations for Capsules 4 and 13 just prior to end of Phase IV Part 1**

Capsule	Initial pellet-clad clad-capsule gaps	Temperatures °C				Diametral gap (mil)		Pellet-clad contact during irradiation
		Pellet centerline	Pellet mean	Clad wall	Capsule wall	Pellet-to-clad	Clad-to-capsule	
4	Minimum	884	613	219	97.7	0.51	1.79	Never
	Maximum	1014	733	247	97.6	1.02	2.54	Never
13	Minimum	896	619	222	98.3	0.50	1.79	Never
	Maximum	1028	740	250	98.2	1.00	2.54	Never

Although the calculated mean capsule wall temperature is virtually independent of assumptions with respect to the initial pellet-clad and clad-capsule gap widths, the calculated mean clad temperature is higher for the pellets with maximum initial gaps. During reactor operation at the end of Phase IV Part 1, the temperature (about 250°C) of the clad surrounding these pellets is much higher than that (about 98°C) of the capsule wall, where temperature is controlled by forced convection to the coolant flow at the outer surface.

The predicted mean temperature for the pellets with minimum initial gaps is about 616°C, so the fuel thermal expansion is significant. (The calculated pellet centerline temperature is about 890°C.) Nevertheless, with pellet densifications of 2.0 percent, pellet-clad contact is not predicted to occur. As indicated in Table 2.5, the pellet-to-clad diametral gap just prior to reactor shutdown from Cycle 127A is calculated to be about 0.50 mil.

For pellets with maximum initial gaps, Table 2.5 indicates the expected larger (about 1.02 mil) calculated pellet-to-clad gap at the end of the irradiation. Also, since larger gaps imply smaller effective gap conductances, the predicted temperatures for these pellets are higher.

In all cases, no clad contact is predicted at the pellet midplane throughout the irradiation. Thus, locally imposed clad strain is limited to that caused by thermal expansion (about 0.1 percent) and irradiation-induced creep (about 0.2 percent). Table 2.5 indicates calculated clad-to-capsule diametral gaps of between 1.79 and 2.54 mils at the end of the irradiation.

## **2.8 Predicted Conditions for the Capsules in the Hot Cell**

The final burnup advancement steps in each CARTS calculation represent conditions from the time that the capsules arrive at ORNL (April 2002) through the time (July 2002) that the fuel pins are expected to be opened for pellet inspection. For these three final calculation steps, the fuel pins are heated internally by decay power, while heat transfer from the outer capsule surface is by convection to the hot cell atmosphere.

Capsules 4 and 13 were introduced into the ORNL hot cell on April 22, 2002, about six weeks after completion of irradiation and their removal from the test assembly. The MOCUP protocol (coordinating calculations by MCNP and ORIGEN) was applied at INEEL to predict isotopic inventories and decay powers as documented in Reference 11. During the period from mid-April to end-August, these results show that the pellet stack decay power falls from 4.0 to 1.7 watts

# Capsule 13

ORNL 2002-0094C EFG

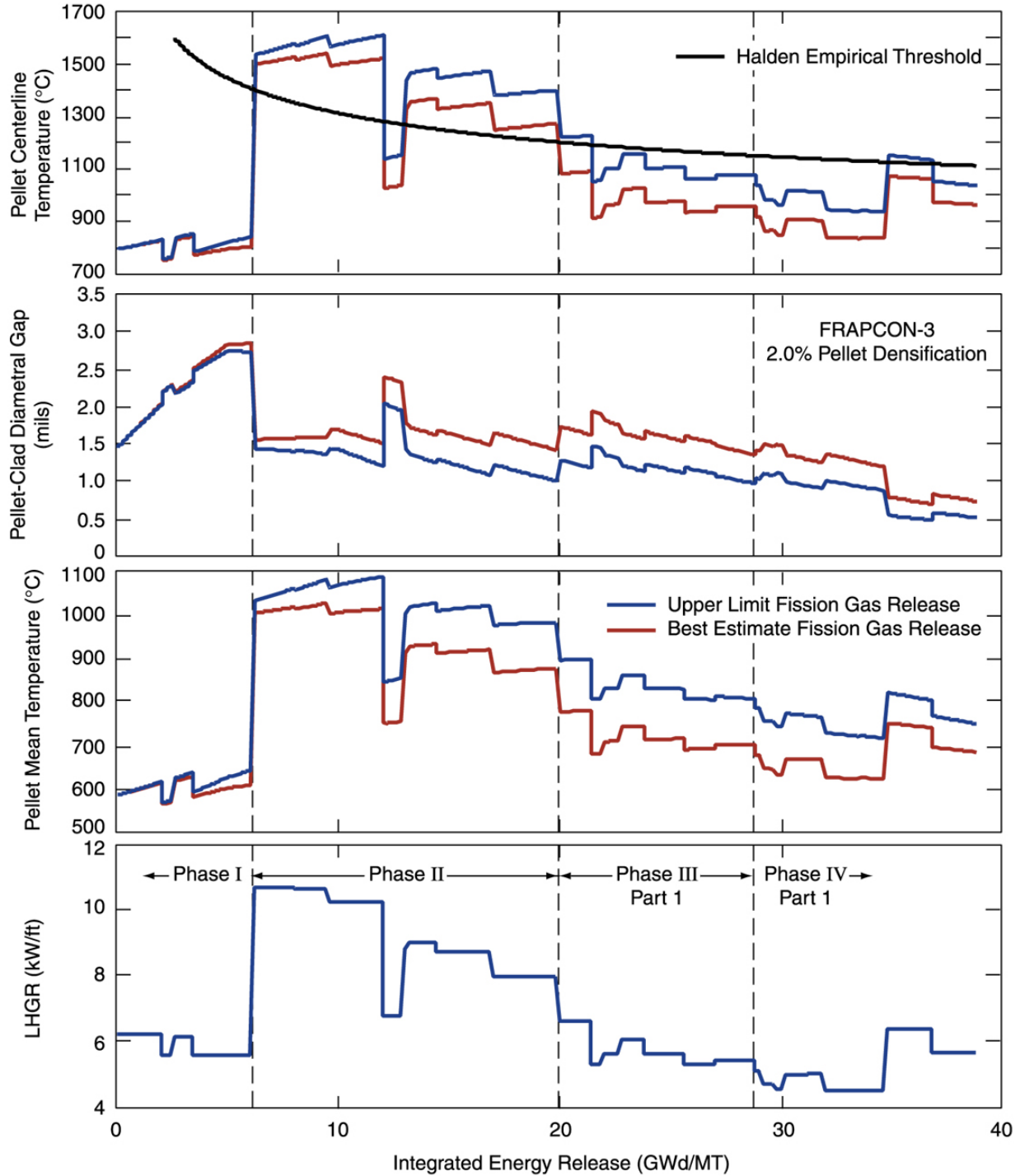


**Fig. 2.5. Comparison of CARTS predictions for Capsule 13 (mean as-built dimensions) showing effects of upper-limit versus best-estimate fission gas release fractions.**

(0.0080 to 0.0034 kW/ft).

The CARTS predictions for the capsule conditions at the expected time of opening are based on a decay power of 2.2 watts (0.0044 kW/ft), which corresponds to mid-July 2002. Heat transfer from the outer capsule surface is by free convection to the hot cell atmosphere. The natural convection heat transfer coefficient based on the capsule surface area directly over the pellet stack has been established as 27.5 W/m<sup>2</sup>-°C (4.77 Btu/hr-ft<sup>2</sup>-°F), based upon temperature measurements for the capsules examined in previous PIEs.

Table 2.6 presents the results of the CARTS calculations for conditions in the hot cell with decay heat corresponding to mid-July 2002. The final column of Table 2.6 indicates the predicted internal pressure within the fuel pins.

**Table 2.6. CARTS predictions for Capsules 4 and 13 under hot cell conditions (mid-July 2002)**

Capsule	Initial pellet-clad clad-capsule gaps	Temperatures °C				Diametral gap (mil)		Fuel pin internal pressure psia
		Pellet centerline	Pellet mean	Clad wall	Capsule wall	Pellet-to-clad	Clad-to-capsule	
4	Minimum	45.6	45.5	44.7	44.6	2.14	1.73	67.9
	Maximum	45.8	45.7	44.8	44.6	3.04	2.53	65.7
13	Minimum	45.5	45.4	44.7	44.5	2.14	1.73	66.4
	Maximum	45.8	45.6	44.7	44.5	3.04	2.53	64.3

For the time of capsule opening, the pellet-to-clad diametral gaps within the fuel pins are predicted to lie between 2.14 and 3.04 mils, a range of 0.90 mil. Within this calculated range, the individual gap widths associated with the 15 different pellets are determined by the relative width of each pellet's initial cold diametral gap, which the design tolerances allow to lie between 2.0 and 3.5 mils.

The pressure within the fuel pins (based on the combined volumes of the pellet-clad annular gap and the gas plenum associated with the actual stack length for these capsules) is predicted to be about 66 psia (51.3 psig). This result is obtained by use of an assumed fission gas (krypton and xenon) release from the fuel matrix in accordance with the best estimate (4.2% at 45 GWd/MT) as discussed in Section 2.6.1.2. About 10.0 psi of the total pressure is contributed by helium created during the irradiation, half of which is assumed released to the fuel pin free volume. The fuel pin pressures measured for the intermediate (21 GWd/MT) and 30 GWd/MT withdrawal capsules were in close agreement with the CARTS predictions.

The diametral gap between the outer surface of the Zircaloy clad and the inner surface of the stainless steel capsule is predicted to lie in the range from 1.73 to 2.53 mils. This range of 0.80 mil strictly follows from the design tolerances, which permitted the cold clad-to-capsule initial diametral gap to vary between 2.2 and 3.0 mils.

## 2.9 Potential for Increased Gas Release Fraction

The gas inventories of krypton, xenon, and helium established by the MOCUP calculations performed at INEEL are listed in Table 2.7. It should be noted that the helium inventory is time-dependent [most is produced via decay (163-day half-life) of Cm-242], and the value listed corresponds to the mid-July expected time of capsule opening.

Although the creation of krypton and xenon is directly proportional to burnup, the helium inventory has increased much more rapidly, slightly more than doubling between 30 and 40 GWd/MT. Although about 70 times more fission gas (Kr and Xe combined) is created, the fractional release of helium to the fuel pin free volume is more than ten times higher.

Furthermore, this released helium is augmented by the helium introduced (at atmospheric pressure) as the initial fill when the fuel pin free volume was closed at Los Alamos. Consequently, the helium partial pressure is about one-third of the fuel pin total.

**Table 2.7. Gas contents within Capsule-4 and -13 fuel as predicted by MOCUP calculations**

Capsule	Gas content, gram atoms x 10 <sup>-5</sup>			
	Krypton	Xenon	Total fission gas	Helium
4	24.66	410.4	435.1	6.22
13	24.61	409.6	434.2	6.27

If the gases listed in Table 2.7 are assumed to have escaped to the fuel pin free volume in accordance with the release fractions observed in the previous (30 GWd/MT) PIE, the resulting total pressure is in the range from 38–48 psia. The European experience shows, however, that the gas release fraction is a function of the highest temperature experienced by the fuel. The peak fuel temperatures in this experiment occurred during the first two cycles of the Phase II irradiation. Since the LHGRs imposed on Capsules 4 and 13 at this time were about ten percent higher than for the capsules withdrawn at 30 GWd/MT, the peak fuel temperatures (shown in Figures 2.1 and 2.4) are correspondingly higher. Accordingly, the gas releases for Capsules 4 and 13 are expected to be higher than the range (1.5%–2.3%) observed in the previous PIE. A concise summary of the interacting phenomena that lead to gas release from the fuel matrix is provided by recent French Researchers (Reference 12) as follows:

“The generally accepted scenario involves an initial intragranular phase during which atomic diffusion of fission gases to the grain boundary is hindered by nucleation of intragranular bubbles, which then act as sinks for diffusing atoms; intragranular nucleation and growth itself being offset by re-resolution of gas atoms from bubbles into the oxide lattice. Eventually, the intragranular gas reaches the grain boundaries at which gas may accumulate to a certain extent thus delaying actual release. Then, above a certain burnup, in fact probably concentration dependent temperature threshold, bubbles nucleate at grain boundaries and grow until they connect up with each other. It is at this stage that venting of fission gases to the plenum begins.”

The “connecting up” or “tunneling” of bubbles opens passages permitting escape of some of the gas to the fuel pin free volume. Obviously, the escape of gases is facilitated when the path length to the free volume is shortened, and this occurs when cracks are opened within the pellet. This MOX test fuel has been subjected to about 50% more thermal cycling than commercial reactor fuel would experience in being irradiated to the same burnup. Hence additional cracking is expected to have occurred, which will tend to facilitate gas release.

As shown in Table 2.6, the best-estimate fission gas release curve, characterized by a 4.2% release at 45 GWd/MT, produces a CARTS-predicted fuel pin pressure of about 66 psia. Subtracting the partial pressure of helium (both initial fill and half of the additional helium created during irradiation), the fission gas partial pressure is about 45.5 psi. Based on the fuel gas content inventories shown in Table 2.7, this is equivalent to a fission gas release fraction of 3.7% for Capsules 4 and 13. This is somewhat higher than the range (1.5%–2.3%) obtained in the previous PIE, but for the reasons expressed above, such an enhanced release behavior is believed reasonable.

Finally, CARTS predictions obtained for an upper-limit fission gas release of 16.5% for Capsule 4 and 16.9% for Capsule 13 are shown in Figures 2.2 and 2.5, respectively. The corresponding fuel pin total pressure at the time of opening would be approximately 196 psia, which is three times higher than the 66 psia associated with the best-estimate gas release as listed in Table 2.6.

## **2.10 Summary and Conclusions from the CARTS Predictions**

For Capsules 4 and 13 with burnups of 39.9 GWd/MT, the CARTS code predicts that the 15 pellets within each fuel pin will exhibit, under hot cell conditions, individual pellet-to-clad diametral gap widths ranging from 2.14 to 3.04 mils. (Where internal cracks are present, the diametral gap is defined to include the width of these open cracks.)

Clad contact at the pellet midplane is not predicted to have occurred at any time during the irradiation. However, progressively increased clad diameters have been observed in the previous PIEs. This outward movement of the cladding adjacent to the pellet midplane is believed due to irradiation-induced creep under the impetus of internal gas pressure and, more importantly, local tensile stress mechanically imposed by hourglassing at the pellet interfaces. Since the fuel pin and capsule were initially filled with helium at atmospheric pressure, the differential pressure across the clad wall is initially very small, due only to the higher temperature of the gas in the fuel pin. However, the fuel pin internal pressure increases with burnup due to fission gas release and the wall hoop stress imposed by pressure differential approaches four MPa as burnup increases to 50 GWd/MT.

Pellet hourglassing imposes a high hoop stress at clad locations overlying the pellet interfaces. As discussed in Chapter 6 of Reference 13, yielding and plastic deformations occur within narrow bands directly overlying the clad contact points at the pellet ends. Mechanical stretching in response to the clad lifting at the interfaces places the clad at the pellet midplanes in tension. The stress magnitude at the pellet midplanes depends upon the extent of clad plastic deformation at the pellet ends and the clad hardness, which increases with irradiation. For the current

calculations, the permanent clad deformation imposed by irradiation-induced outward clad creep is represented as 0.59 mil, a 0.18% increase in fuel pin outer diameter.

The diametral gap between the fuel pin and capsule is predicted to lie between 1.73 and 2.53 mils, which may be compared to the range of 2.2–3.0 mils for the initial cold capsule conditions. These results suggest that fuel pin removal from the capsule and the subsequent fuel pin disassembly should be straightforward, without significant interference from either pin-to-capsule or pellet-to-clad binding.

Based on the best estimate for gas release from the fuel matrix, the gas pressure within the fuel pin when opened in the hot cell is predicted to be about 66 psia (51.3 psig). There are two factors, however, that might serve to increase the gas release fraction for these capsules. First, the LHGRs experienced during this test irradiation are somewhat higher than those normally encountered in the literature, and higher fuel temperatures tend to increase the extent to which fission gas escapes from the fuel. Second, these fuel pellets have experienced 42 thermal cycles, about half again as many as would be expected for normal reactor operation to this burnup. Thus, the gas release may have been facilitated by a greater-than-normal extent of pellet thermal cracking.

### 3. “QUICK LOOK” PRELIMINARY PIE

Table 3.1 details the items that have been selected for Step I of the PIE effort. Note that these items form a subset of the total PIE. The capsules made available for the 40 GWd/MT PIE effort are Capsule 4 (fuel prepared without gallium removal) and Capsule 13 (fuel for which the PuO<sub>2</sub> was treated for gallium removal).

**Table 3.1. Quick Look Metrology**

No.	Examination	Comments
1	Capsule photo visual	Containment integrity is major interest.
2	Capsule temperature measurement	Compare measured temperatures with predictions.
3	Capsule dimensional inspection	Containment integrity is major interest
4	Capsule gamma scan	Determine gross internal state of capsule and fuel pin.
5	Fission gas sampling	The fission gas pressure and <sup>85</sup> Kr content of both the containment and the fuel pin will be analyzed.
<i>Remove fuel pin from capsule</i>		
6	Fuel pin photo	First assessment of clad integrity.
7	Fuel pin dimensional inspection	Detailed assessment of clad integrity and local deformation caused by pellet-clad contact.
8	Fuel pin gas free volume measurement	Determine the total free volume within the fuel pin.

Note that the capsule and fuel pin numbering are not the same; Table 3.2 details the relationship between the two and identifies the status with respect to gallium removal treatment.

#### 3.1 Capsule Photo Visual Inspection

The first portion of the PIE effort was to visually examine the capsule surfaces at low magnification. The capsules were not as clean and bright as previous capsules were. There appeared to be more handling scratches and some mild discoloration, but no physical distortions or damage. This is not unexpected as both capsules have been in the reactor a long time. In general, the stainless steel containment survived the irradiation as expected and these capsules appear similar to the capsules previously removed at 8, 21, and 30 GWd/MT.

Photographs of these capsules are shown in Figures 3.1 through 3.6 for a variety of views. The two appear identical except for the identification marks. The black lines near the welding border are the heat-affected zone and are unrelated to the irradiation. While not obvious from a comparison of the photographs shown in Figures 3.1 and 3.4, when held side-by-side both capsules have an equal amount of surface discoloration in the same location (overlying the fuel stack). The nature of this discoloration will be determined during the remainder of the PIE.

**Table 3.2. Capsule and Fuel Pin Numbers**

<b>Capsule Number</b>	<b>Fuel Pin Number</b>	<b>Fuel Batch</b>	<b>Gallium Treatment</b>	<b>Exposure (GWd/MT)</b>	<b>PIE Status</b>
1	2	A	None	8	Complete –Pending clad ductility testing
2	5	A	None	21	Complete –Pending clad ductility testing
3	6	A	None	30	Complete –Pending clad ductility testing
4	7	A	None	40	Underway – Subject of this report
5	8	A	None		In Reactor
6	9	A	None		In Reactor
7	10	A	None		Archive
8	11	B	Thermal (TIGR)	8	Complete –Pending clad ductility testing
9	12	B	Thermal (TIGR)	21	Complete –Pending clad ductility testing
10	13	B	Thermal (TIGR)	30	Complete –Pending clad ductility testing
11	14	B	Thermal (TIGR)		Archive
12	15	B	Thermal (TIGR)		In Reactor
13	16	B	Thermal (TIGR)	40	Underway – Subject of this report

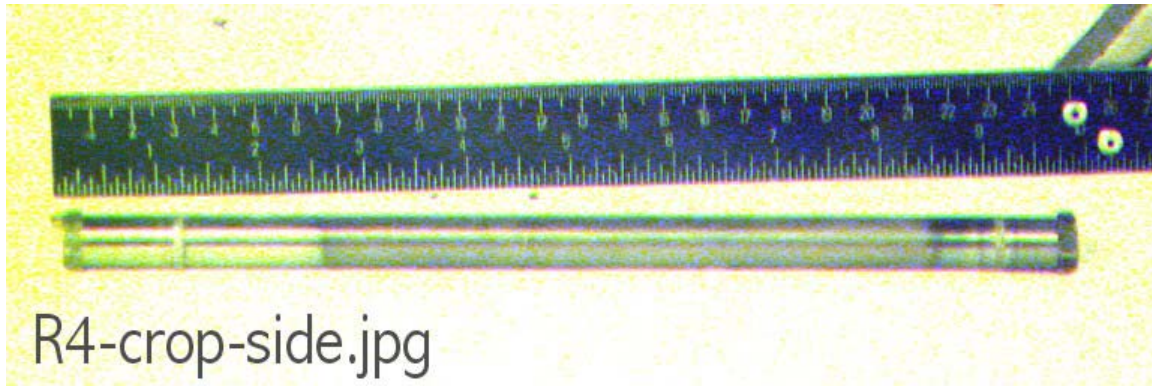


**Figure 3.1. Side view of Capsule 4. Note the discoloration on the right 2/3<sup>rd</sup> of the capsule.**



**Figure 3.2. Top view of Capsule 4.**

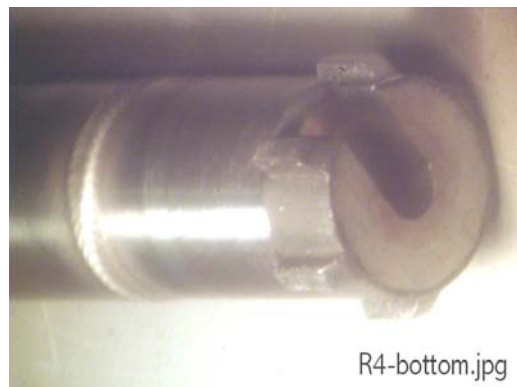


**Figure 3.3. Bottom view of Capsule 4.**

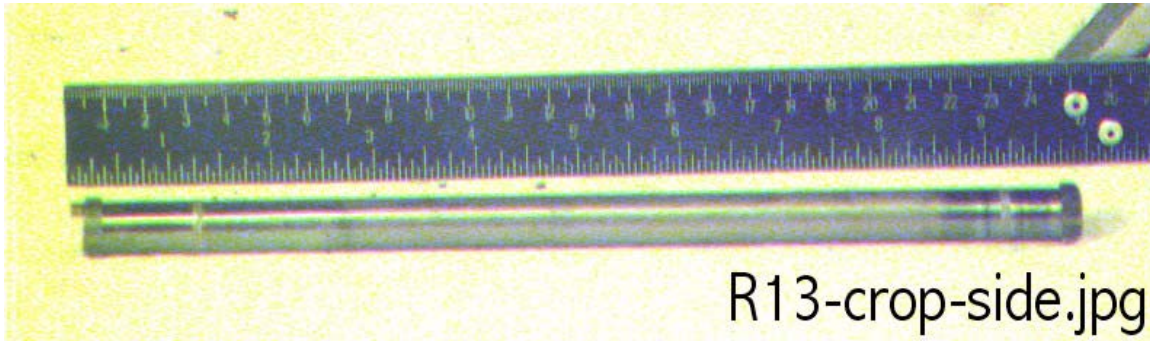
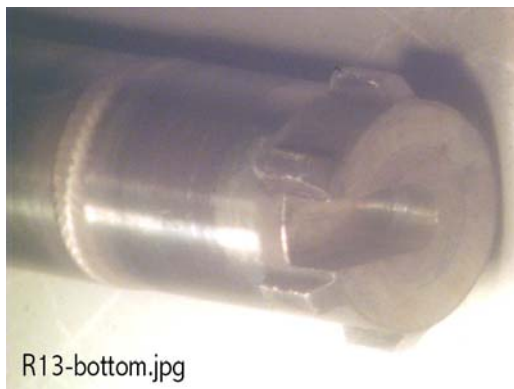


**Figure 3.4. Side view of Capsule 13. The discoloration is similar to that on Capsule 4.**



R13-top.jpg

**Figure 3.5. Top view of Capsule 13.**



R13-bottom.jpg

**Figure 3.6. Bottom view of Capsule 13.**

### 3.2 Capsule Temperature Measurements

The temperature measurements and their locations as taken on Capsules 4 and 13 are shown in Table 3.3. A photo of a capsule undergoing a measurement is shown in Fig. 3.7. The apparatus consists of a Type C thermocouple held to the capsule by a modified hose clamp.

**Table 3.3. Capsule 4 and 13 Temperature Measurements**

<b>MOX Capsule 4</b>	
<i>Measurements taken on 04/25/2002</i>	
Top Weld	42.7°C
Mid Point	56.5°C
Bottom Weld	48.2°C
<i>Average</i>	<i>49.1 °C</i>
Cell Ambient	30.0°C
<b>MOX Capsule 13</b>	
<i>Measurements taken on 04/26/2002</i>	
Top Weld	40.2°C
Mid Point	56.8°C
Bottom Weld	46.3°C
<i>Average</i>	<i>47.8 °C</i>
Cell Ambient	29.8°C

Notes:

*Capsule temperature measurements were taken approximately 12" from the hot cell tabletop and allowed to stabilize for 45 minutes. These values are used to set the capsule surface heat transfer coefficient, as discussed in Section 2.8.*

### 3.3 Capsule Dimensional Inspection

The results of the stainless steel capsule dimensional inspections are shown in Table 3.4. Within 0.001 inches, there were no indications of bowing or out of roundness. Measurements for bowing were carried out between the capsule welds. Only a slight difference between pre- and post-irradiation diametrical values was noted, 0.001 inches or less, which is attributed to the thermal expansion associated with the somewhat higher measurement temperatures in the hot cell. The lengths of the capsules were found to agree with the preirradiation values within 0.01 inches. Figure 3.8 details the measurement method for diametrical dimensions.

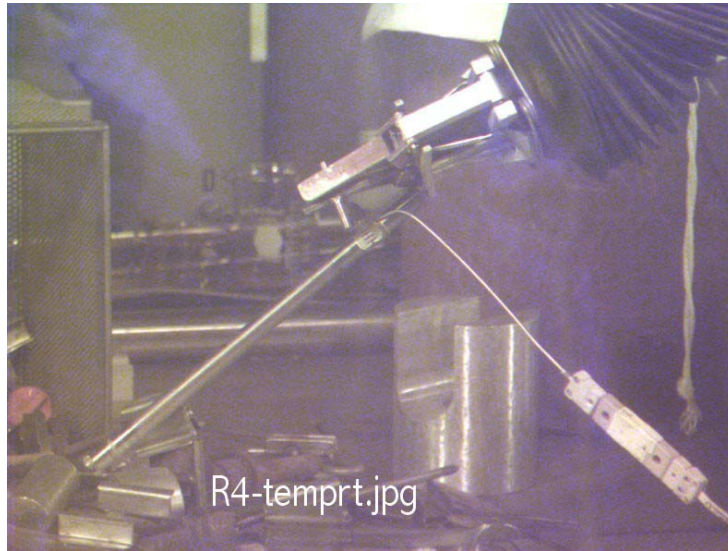


**Figure 3.7. Free air temperature measurement on Capsule 4.**

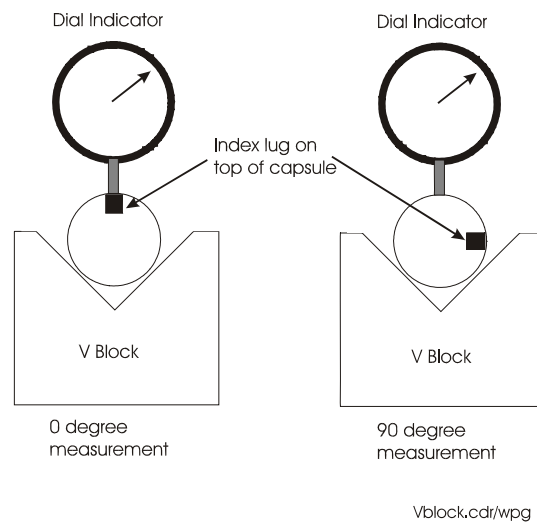


**Figure 3.8. Schematic of diameter measurement.**

**Table 3.4. Capsule Measurements**

Approximate Axial Location	Diameter Measurements (in) (±0.0005 in)		Preirradiation Value (Room Temperature) (in)
	0°	90°	
<b>Capsule 4</b>			
3.8" from capsule top	0.4652	0.4654	0.4643 to 0.4649
Center of capsule	0.4655	0.4655	
5.8" from capsule top	0.4655	0.4659	
<b>Capsule 13</b>			
3.8" from capsule top	0.4654	0.4653	0.4643 to 0.4649
Center of capsule	0.4655	0.4654	
5.8" from capsule top	0.4655	0.4654	
<b>Length (in) (±0.005 in)</b>			
<b>Capsule 4</b>	9.585		9.575 after welding (9.59 before welding)
<b>Capsule 13</b>	9.584		9.576 after welding (9.59 before welding)
<b>Mass (g) (±0.1 in)</b>			
<b>Capsule 4</b>	192.2		Not given
<b>Capsule 10</b>	192.5		Not given

### 3.4 Capsule Gamma Scans

Both Capsules 4 and 13 were raster-scanned to obtain a two dimensional view of the capsule internal structure. These scans comprise 6000 points and were taken with a 0.040" diameter collimator in two energy ranges. The range 400 to 700 KeV was employed to broadly cover the fission products while the range 800 to 1575 keV was used to broadly cover the activation products. These two energy ranges were selected because they show the most details of interest for a general view.

In addition, both capsules underwent an axial line scan (400 points) along their length using the same collimator as was used in the two-dimensional scans. Results from these two energy ranges are presented in the following Sections. Overall, the capsules appeared to be intact with no unusual structure or abnormalities.

#### 3.4.1 Capsule 4 Gamma Scan

Figure 3.9 shows the result of the 400 to 700 KeV raster scan for Capsule 4. When compared to the schematic above, one can make out the stainless steel end caps, the fuel pin end caps, and very clearly, the fuel pellet stack. The pedestal at the base of the lower fuel pin end plug is vaguely outlined as well as is the capsule boundary (the capsule bottom is to the left, the top to the right).

The Nominal Fuel Pin Schematic Has Been Shifted Within the Capsule and the Fuel Stack and Spring Scaled to Model the Scan

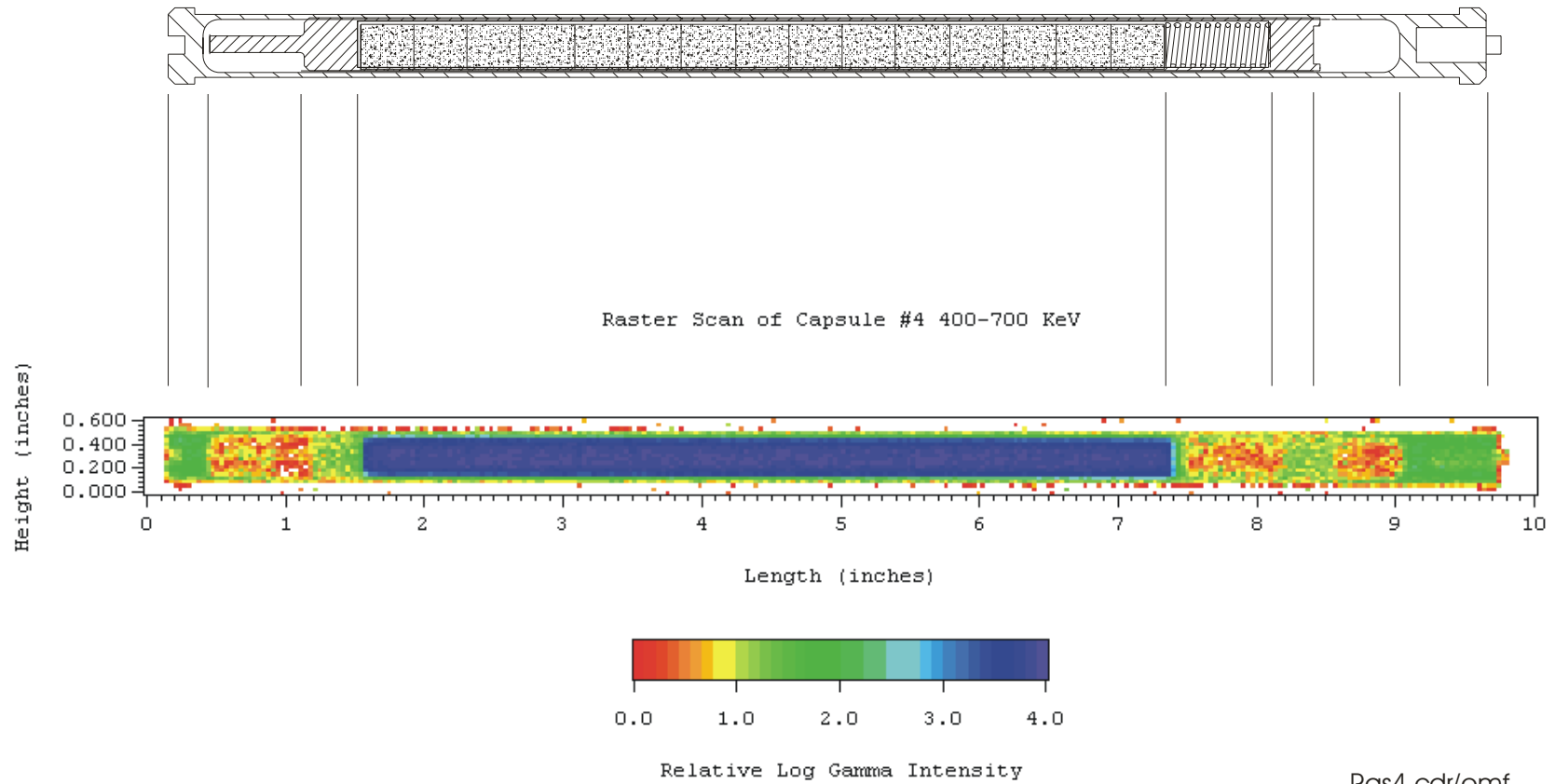


**Figure 3.9. Capsule 4 mid energy gamma raster scan.**

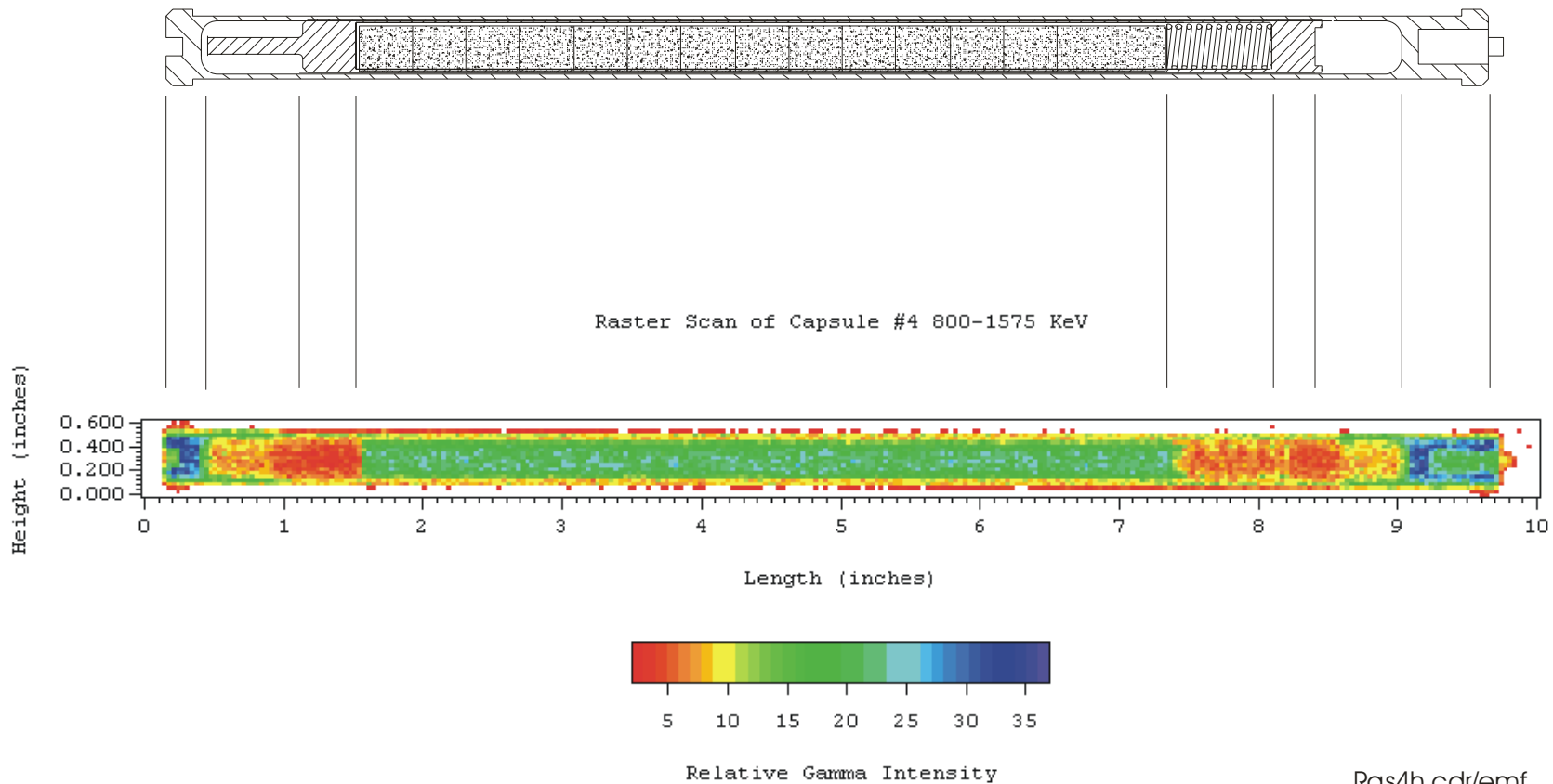
Figure 3.10 shows the raster scan for Capsule 4 in the 800 to 1575 keV energy range. This higher energy range outlines the stainless steel components to a greater degree.

Figure 3.11 shows an axial line scan along the capsule in the 400 to 700 keV energy range. Again, the elements of the capsule are clearly indicated. The fuel pellet stack appears to be about 5.85 inches long, within the apparatus measuring tolerance of the as-built dimension (5.82 inches). The nearly constant activity level along the pellet stack corresponds to the average of the ATR flux shapes at the positions within the test assembly where this capsule was located during the irradiation, and is as predicted by the neutronic codes.

Figure 3.12 shows an axial line scan in the energy range of 800-1575 KeV, which accents the stainless steel activation products. This figure shows the stainless steel capsule end caps and wall more clearly. The fuel can be seen because of the high-energy fission product emitters such as  $^{140}\text{La}$ .

Overall, the capsule showed no structural problems. All components appeared to be in their proper locations and the fuel pellet stack does not appear to have swelled significantly.

The Nominal Fuel Pin Schematic Has Been Shifted Within the Capsule and the Fuel Stack and Spring Scaled to Model the Scan



**Figure 3.10. Capsule 4 high-energy gamma raster scan.**

The Nominal Fuel Pin Schematic Has Been Shifted Within the Capsule and the Fuel Stack and Spring Scaled to Model the Scan

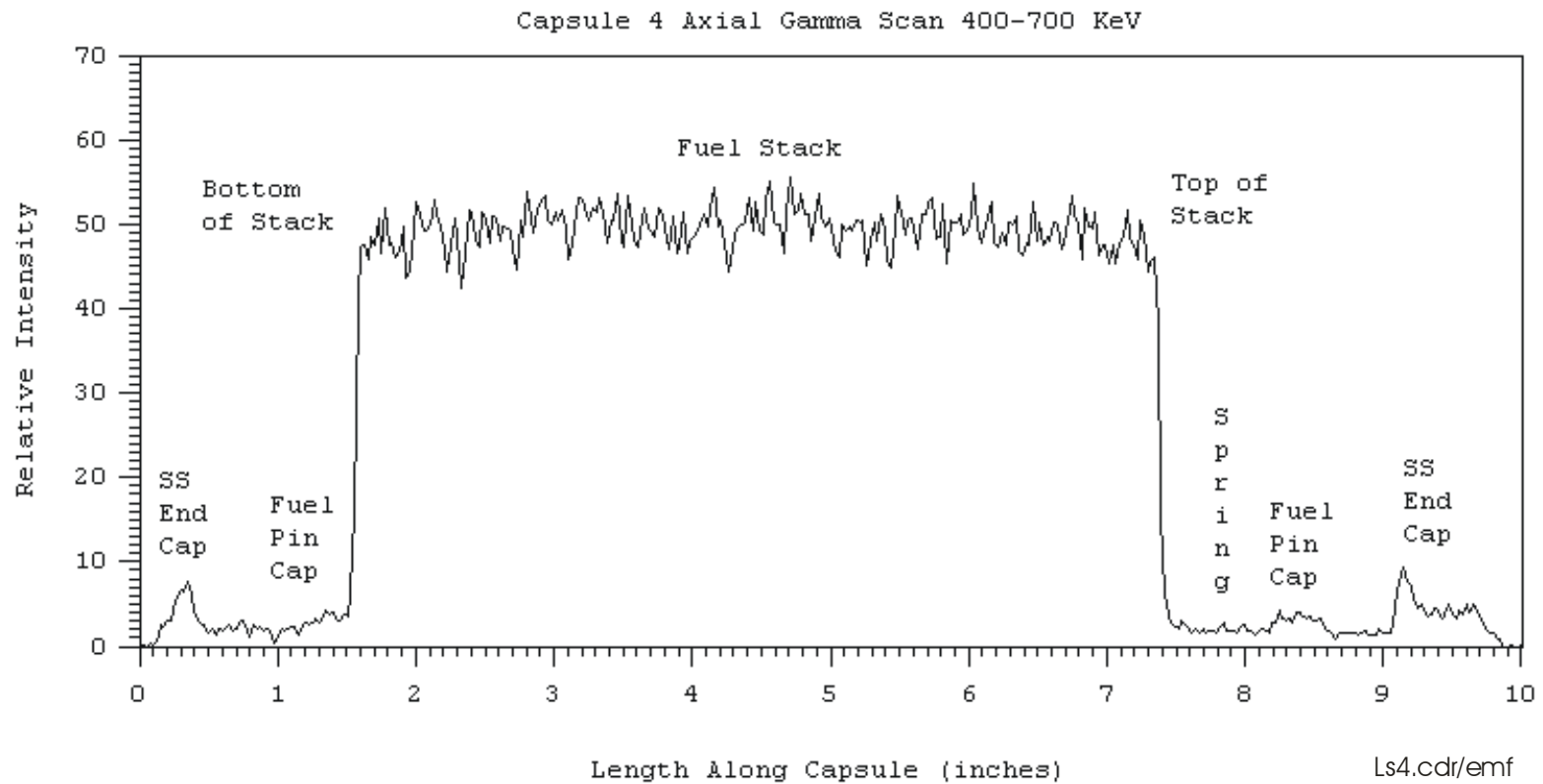
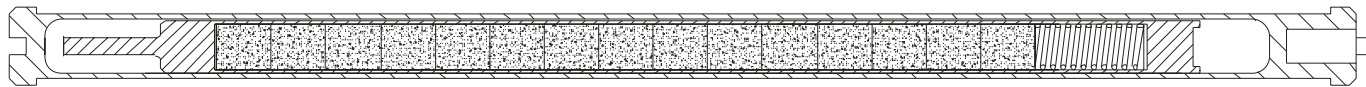


Figure 3.11. Capsule 4 mid energy gamma line scan.



### 3.4.2 Capsule 13 Gamma Scan

Figure 3.13 shows the results of the 400 to 700 keV raster scan for Capsule 13. As before, one can make out the stainless steel end caps, the fuel pin end caps, and the fuel pellet stack. Figure 3.14 shows the same scan in the 800 to 1575 energy range. No inconsistencies or abnormalities in internal component locations were noted.

Figure 3.15 shows an axial line scan along Capsule 13 in the 400 to 700 keV energy range. Again, the elements of the capsule are visible. The fuel stack appears to be approximately 5.8 inches long, which compares well with the as-built measurement of 5.79 inches. Unlike past PIE work, the pellet dish locations could not be discerned in either capsule gamma scan. The fission product activity is also flat along the pellet stack as was seen in Capsule 4.

Figure 3.16 shows an axial line scan in the energy range of 800-1575 KeV, which accents the stainless steel activation products.

Similar to Capsule 4, Capsule 13 appears to have no structural problems and all components appear to be in their proper locations with no significant axial fuel swelling.

The Nominal Fuel Pin Schematic Has Been Shifted Within the Capsule and the Fuel Stack and Spring Scaled to Model the Scan

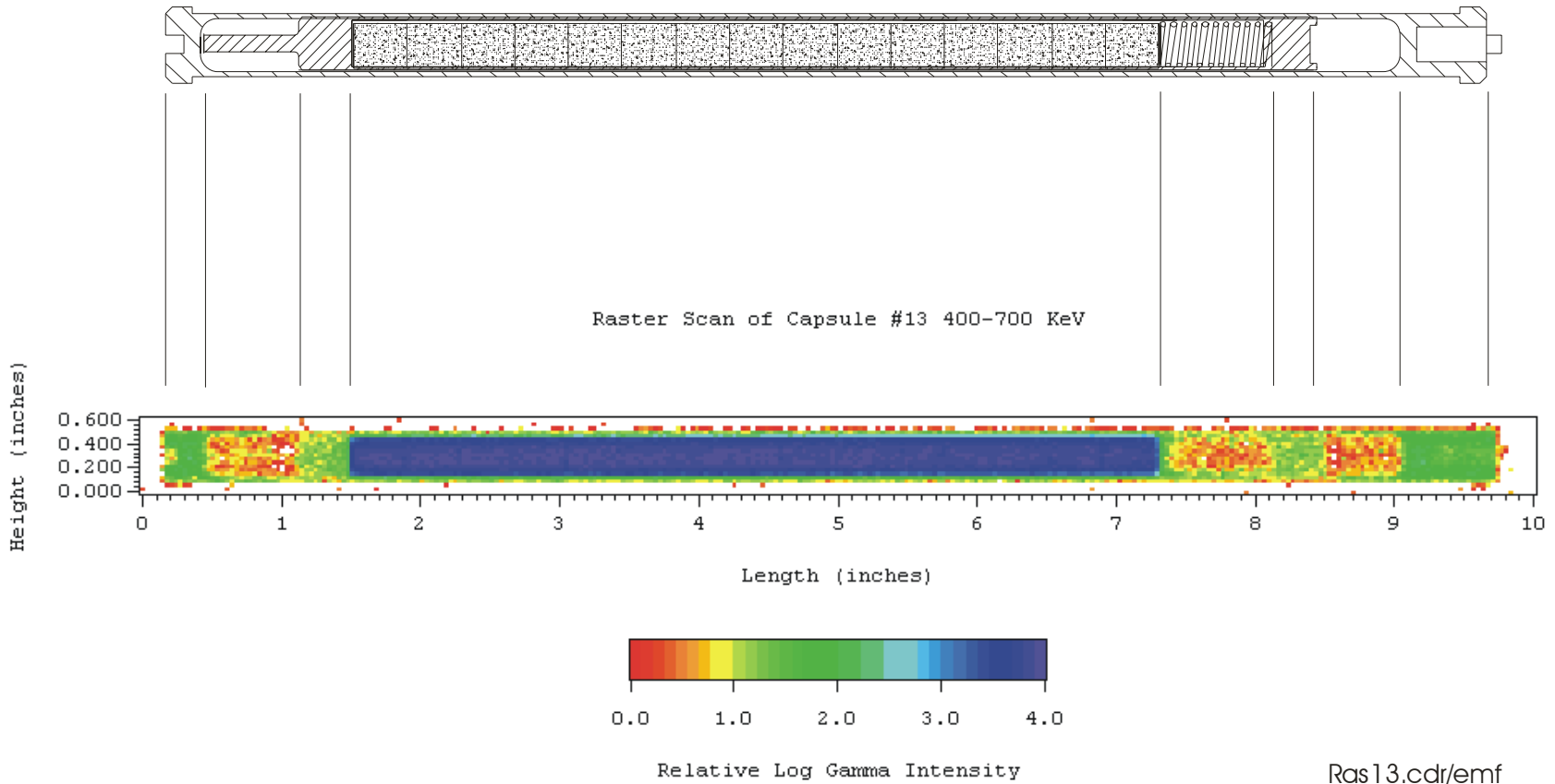


Figure 3.13. Capsule 13 mid energy gamma raster scan.

The Nominal Fuel Pin Schematic Has Been Shifted Within the Capsule and the Fuel Stack and Spring Scaled to Model the Scan

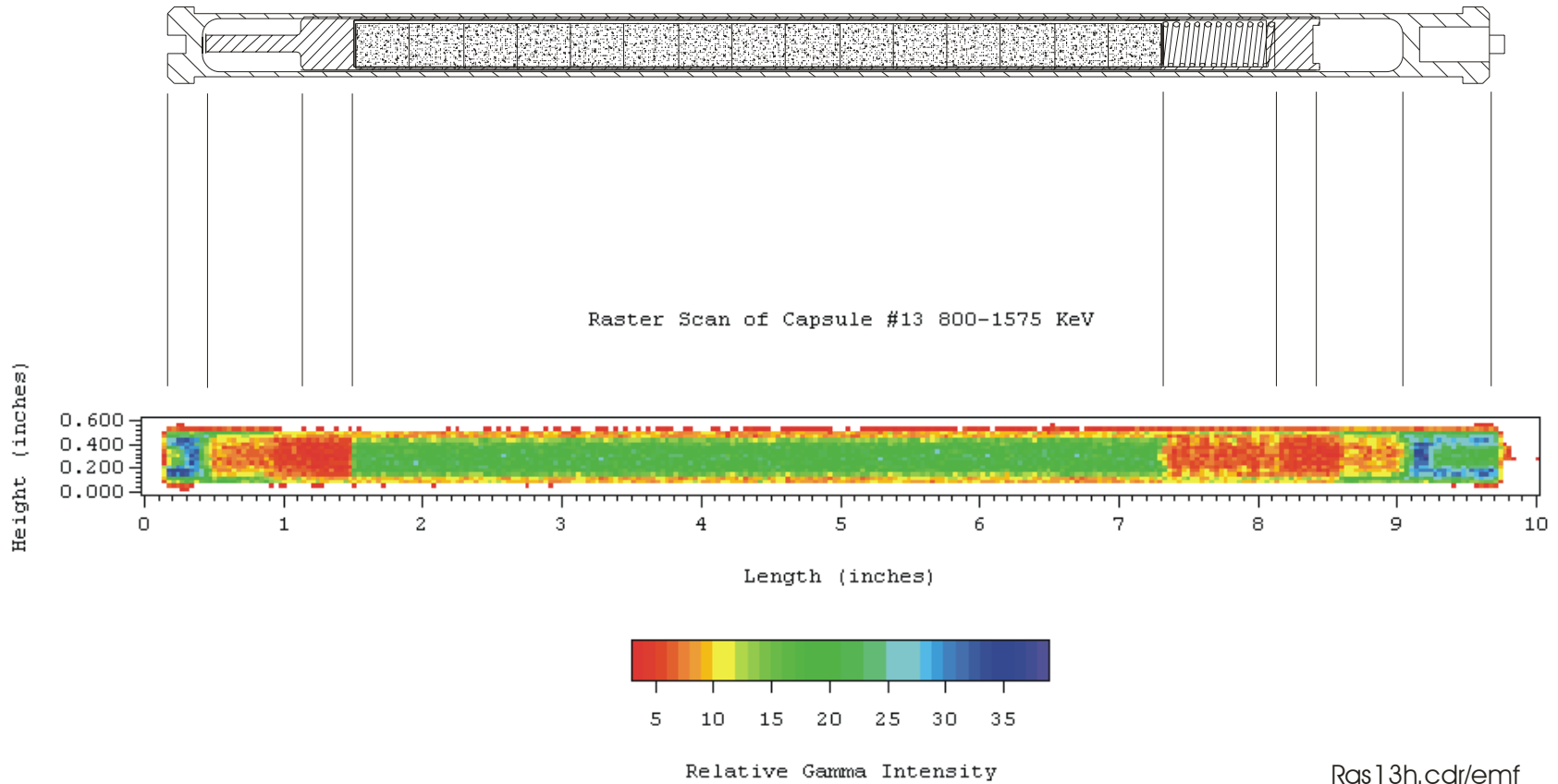
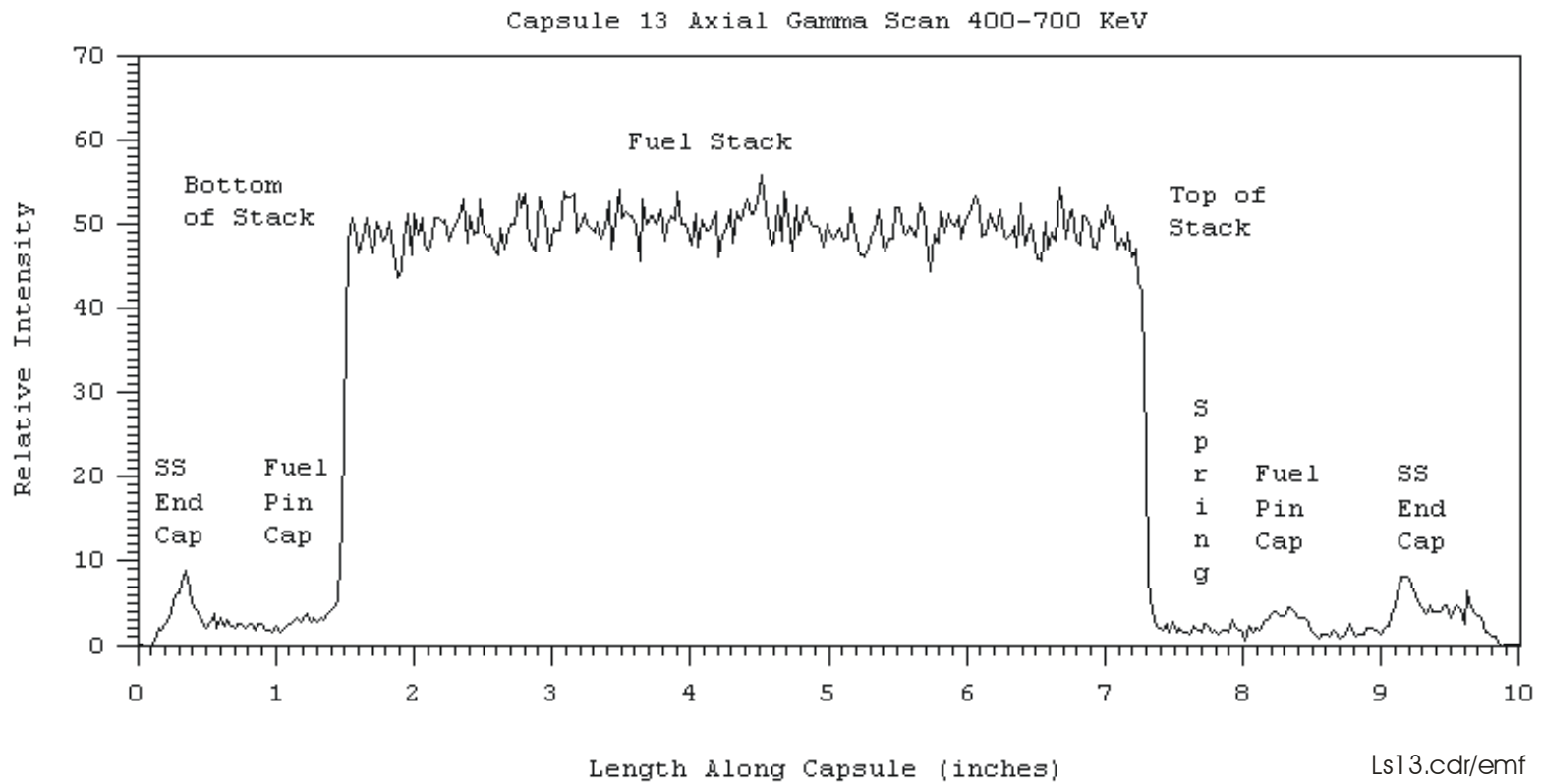
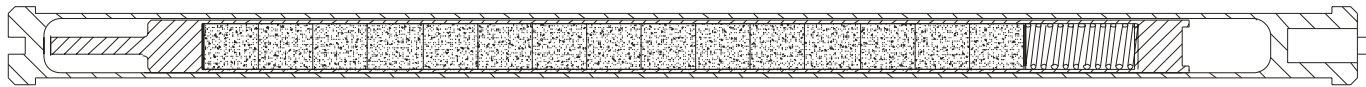


Figure 3.14. Capsule 13 high-energy gamma raster scan.

The Nominal Fuel Pin Schematic Has Been Shifted Within the Capsule and the Fuel Stack and Spring Scaled to Model the Scan



**Figure 3.15. Capsule 13 mid energy gamma line scan.**

The Nominal Fuel Pin Schematic Has Been Shifted Within the Capsule and the Fuel Stack and Spring Scaled to Model the Scan

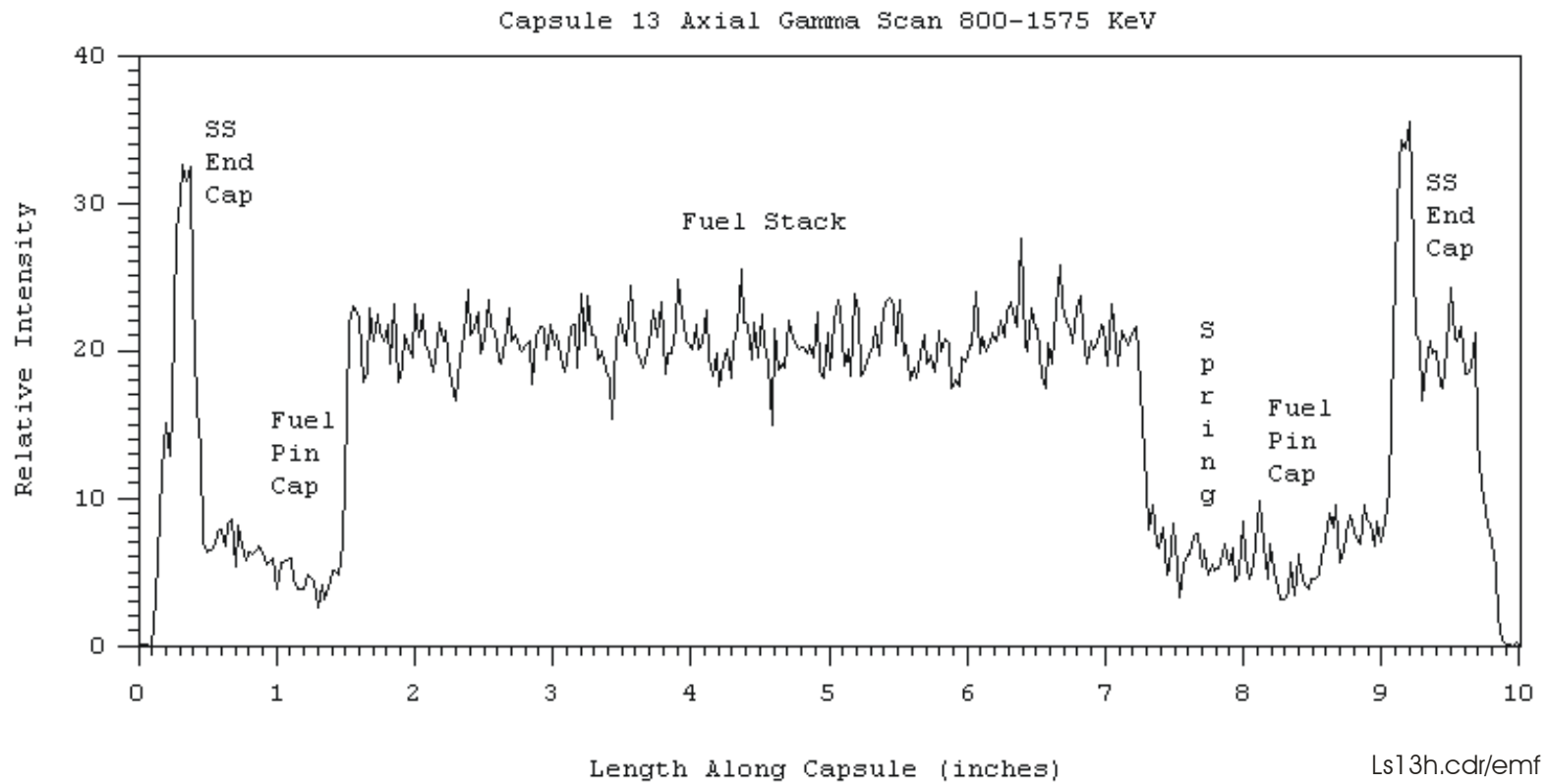
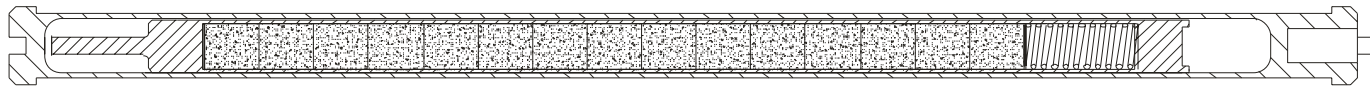
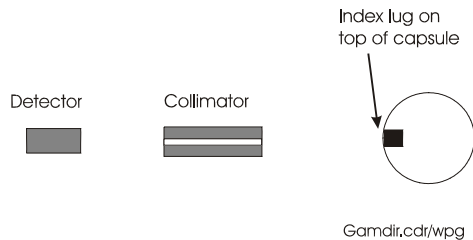


Figure 3.16. Capsule 13 high-energy gamma line scan.

### 3.4.3 Gamma Scanner Data Collection Orientation

The gamma intensity data was collected with the alignment lug of the capsule facing the gamma scanner detector as shown in Figure 3.17.



**Figure 3.17 Orientation of the capsule and the gamma scanner collimator/detector.**

### 3.5 Fission Gas Measurements

The fission gas pressure and  $^{85}\text{Kr}$  content in both Capsules 4 and 13 and their associated fuel pins were measured by use of the MOX Fission Gas Pressure Measuring Apparatus. Details of this apparatus and its calibration are described in Reference 14 and the first use of the device was in the PIE of the 21 GWd/MT capsules [Reference 5]. Briefly, the apparatus functions by using a vacuum sealed drill-press type action to drill first through the trimmed off top of the MOX capsule and then, after sampling the gas in the capsule upper plenum region, to continue drilling into the contained fuel pin. The drilling stops as each barrier is penetrated to permit measurement of the gas pressure and sweeping of the released gases through a cold trap system to trap and determine the  $^{85}\text{Kr}$  quantity. A diagram of the device is shown in Figure 3.18.

The drilling proceeded as planned for Capsule 4, but the drill bit broke before the fuel pin could be punctured in Capsule 13. To recover, Fuel Pin 16 was removed from its capsule, most of the drill fragments extracted from its top cap, and the fuel pin alone remounted. The drill bit in the apparatus was replaced by a mill bit and the weld on the top of the fuel pin was machined away until the seal was broken. The gas release took considerably longer (~2 hours vs. a few seconds) than normal, but no other problems were encountered. The gas was collected in the usual manner.

No anomalous fission gas release was observed in either capsule. The capsule pressures were subatmospheric, as expected since they were sealed at the elevation of INEEL, where the atmospheric pressure is about 12.5 psia. (The actual pressure in the capsule during welding could not be recorded.) The fuel pins were found to be sealed and the fission gas release was found to be in the range of 6.2 to 6.8% (based on  $^{85}\text{Kr}$ ). No problems occurred with the apparatus. The details are summarized in Table 3.5.

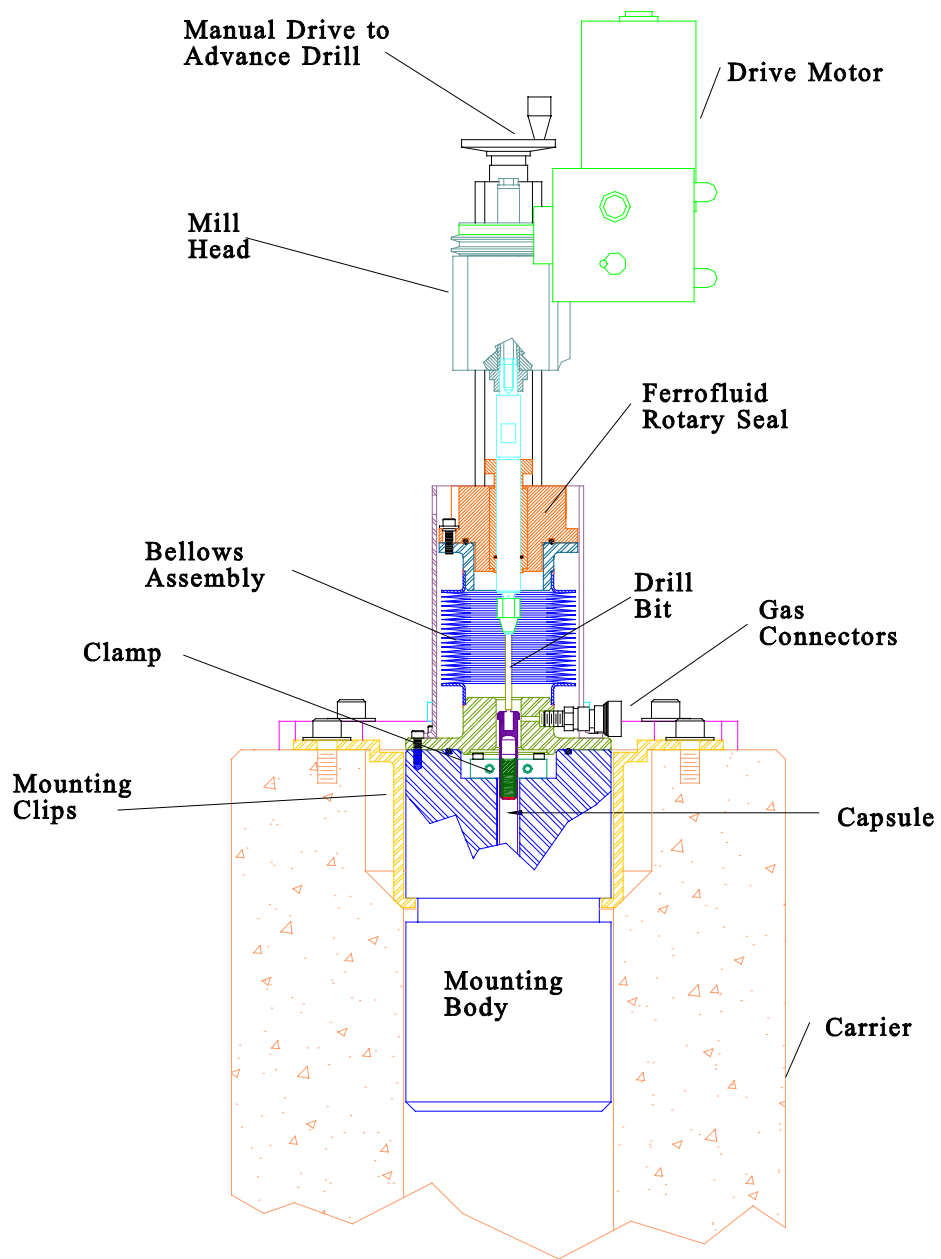


**Figure 3.18. Cross sectional view of the Fission Gas Pressure Measuring Apparatus.  
[Drill Schematic 3.wpg]**

**Table 3.5. Fission Gas Measurements**

<b>Item</b>	<b>Best Estimate Free Volume<sup>1</sup> (cc)</b>	<b>Measured Pressure (psia)</b>	<b>Measured <sup>85</sup>Kr in Free Volume (mCi)</b>	<b>Best Estimate for Total <sup>85</sup>Kr Inventory<sup>2</sup> (mCi)</b>	<b>Model Predicted Pressure<sup>3</sup> (psia)</b>	<b>Release Fraction Based on <sup>85</sup>Kr Measurement</b>
Capsule 4	2.397	10.1	0.00	0	N/A	N/A
Fuel Pin 7	1.339	117.7	31.1	502	67.9	0.062
Capsule 13	2.397	10.2	0.00	0	N/A	N/A
Fuel Pin 16	1.304	143.8	33.9	497	66.4	0.068

<sup>1</sup>Based on as-built dimensional measurements (capsule), volume measurements (Fuel Pin 7), and code predictions (Fuel Pin 16)

<sup>2</sup>Based on ORIGEN calculations (Reference 11) for the time of drilling

<sup>3</sup>Based on CARTS calculations with an estimated release fraction corresponding to 4.5% at 50 GWd/MT, minimum pellet-clad gaps, and nominal fuel pellet stack length dimensions (Chapter 2)

Ambient temperature approximately 23°C

Measured values are approximately ±5% for pressure and ±8% for <sup>85</sup>Kr

### 3.6 Fuel Pin Photo Visual Inspections

Fuel Pin 7 was removed from Capsule 4 by cutting off the bottom of the capsule just above the weld. For this PIE a different technique was used to avoid cutting off the pedestal at the base of the fuel pin. After deburring the capsule body, the fuel pin was removed by grasping and pulling on the full-length pedestal. The pin slid out without difficulty. After removal, the pin was photographed and measured. The exterior of Fuel Pin 7 was found to be in excellent condition.

No attempt was made to maintain the angular orientation of the fuel pin relative to the capsule index lug because the fuel pin is not locked within the capsule during irradiation. Photographs of the fuel pin are shown in Figures 3.19 through 3.21.

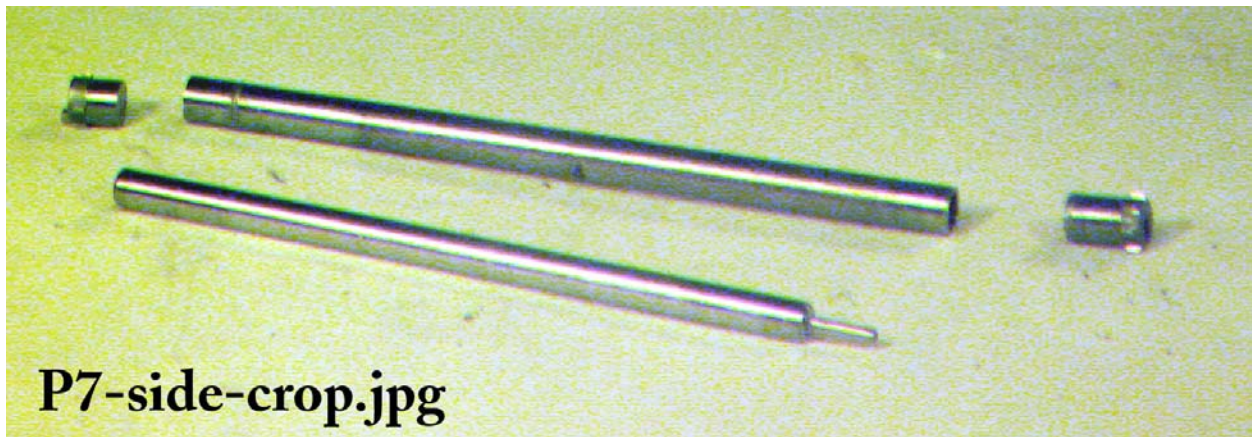


**Figure 3.19. Side view of Fuel Pin 7 (foreground). Shown in the background are the components of the capsule.**



**Figure 3.20. Top view of Fuel Pin 7. The puncture hole can be seen.**

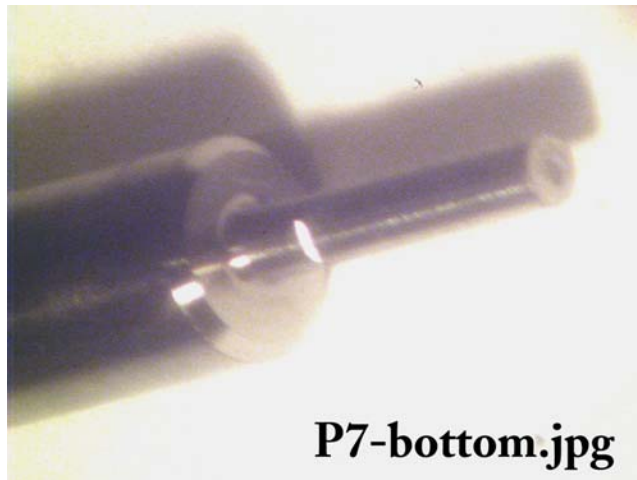


**Figure 3.21. Bottom view of Fuel Pin 7. The vertical mark on the pedestal is a nick made when sawing the capsule bottom off.**

Fuel pin 16 was removed from Capsule 13 in the same manner that Fuel Pin 7 was removed from Capsule 4. Slightly more force was required to pull the pin free. The exterior of Fuel Pin 16 was found to be in excellent condition. Photographs of Fuel Pin 16 are shown in Figs. 3.22 through 3.24.

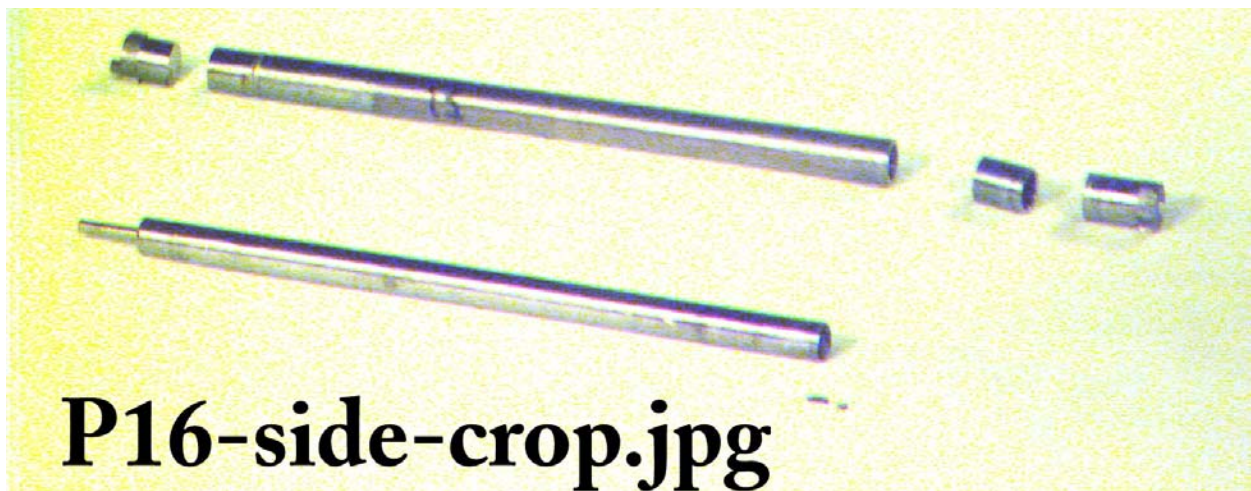


**Figure 3.22. Side view of Fuel Pin 16 (foreground). Shown in the background are the components of the capsule. The small cut off piece of the capsule was used as a spacer when resolving the broken drill problem.**

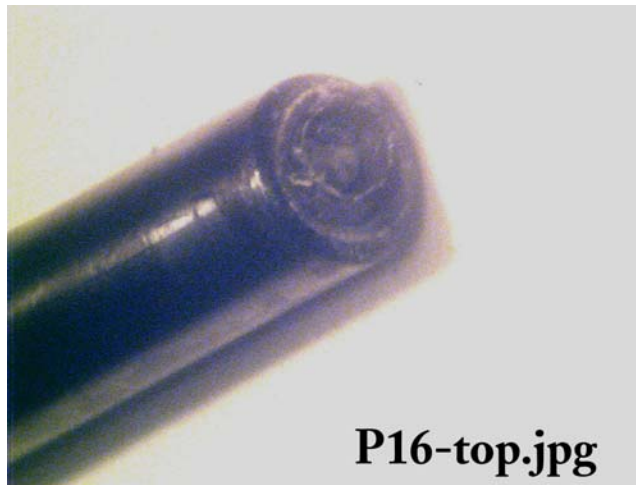


**Figure 3.23. Top view of Fuel Pin 16. A piece of the broken drill bit can be seen in the partially drilled hole.**



**Figure 3.24. Bottom view of Fuel Pin 16.**

### **3.7 Fuel Pin Dimensional Inspections**

The results of the Fuel Pin 7 dimensional inspections are shown in Figure 3.25. These continuous profile measurements were taken using the Fuel Pin Measuring Apparatus (FPMA) as detailed in Reference 15. Accuracy is estimated to be  $\pm 0.1$  mil. The zero reference point is the bottom of the pin; the pedestal region is not measured. The profile as measured for Fuel Pin 16 is shown in Figure 3.26.

A first set of FPMA readings was taken for Fuel Pin 16 in late September. This is the only fuel

pin for which the profile was measured while the pin remained internally pressurized. Similar to Pin 7, both outward clad expansion and clad primary ridges are evident. Pin 16 was found to have a slightly larger mean diameter (0.3820”) than Pin 7 (0.3815”), which tends to explain the additional force required when Pin 16 was extracted. There is no indication of surface discoloration, either in the area over the pellets (where the capsule surface was discolored), or elsewhere.

After Fuel Pin 16 was opened (as described in Section 3.5), a second set of clad profile measurements to determine the average diameter in the absence of internal pressurization was taken in early November. As expected, the average diameter over the fueled region was slightly smaller, 0.3818 Vs 0.3820 for the pressurized case. (The internal pressure of about 144 psia had maintained a small wall tensile stress of about 5.5 MPa after the pellet shrank away from the clad as the pin cooled after irradiation.)

Other than a decrease of 0.20 mil in average diameter, the peaks and valleys of the clad profiles are virtually identical in the two measurements. Thus, an excellent reproducibility of the clad profile measurements has been demonstrated.

There is clear evidence of primary ridging and outward clad creep as was seen in earlier PIEs and predicted by the ABAQUS pellet hourglassing calculations. Any out-of-roundness, bowing (as judged by the fact that the fuel pins could be removed from the tight fitting capsule), and bambooing are insignificant. Other Fuel Pin 7 and 16 measurements are recorded in Table 3.6.

**Table 3.6. Fuel Pin 7 and 16 Length and Weight**

<b>Fuel Pin</b>	<b>Length (in) Less Pedestal ±0.005</b>	<b>Preirradiation Length (in) Less Pedestal</b>	<b>Mass (g)</b>	<b>Preirradiation Mass (g)</b>
<b>Fuel Pin 7</b>	7.411	7.41	111.5	Not given
<b>Fuel Pin 16</b>	7.413	7.41	112.6	Not given

### 3.7.1 Fuel Pin Volume Measurement

After inspection, the free volume of Fuel Pin 7 was measured by using the Fuel Pin Volume Measuring Apparatus detailed in Reference 16. A schematic view of the apparatus is shown in Figure 3.27. This was the first use of this device, which makes use of a simple gas compression technique and a precision pressure gauge to provide a moderate (1%) precision measurement of the fuel pin free volume.

The free volume within a fuel pin is determined by placing the (drilled) opened pin in an apparatus with a changeable volume (piston and cylinder) and measuring the pressure of the system both before and after the known change in volume. A big advantage of this compact design is that there are no valves, gas fill lines, or vacuum lines and it can be easily calibrated with a set of known volumes.

The measured free volume is shown as an entry in Table 3.5 and was used when computing the gas pressure. Because of the drilling problems, the free volume of Fuel Pin 16 could not be measured.

Fuel Pin 7 Average Diameter Measurement

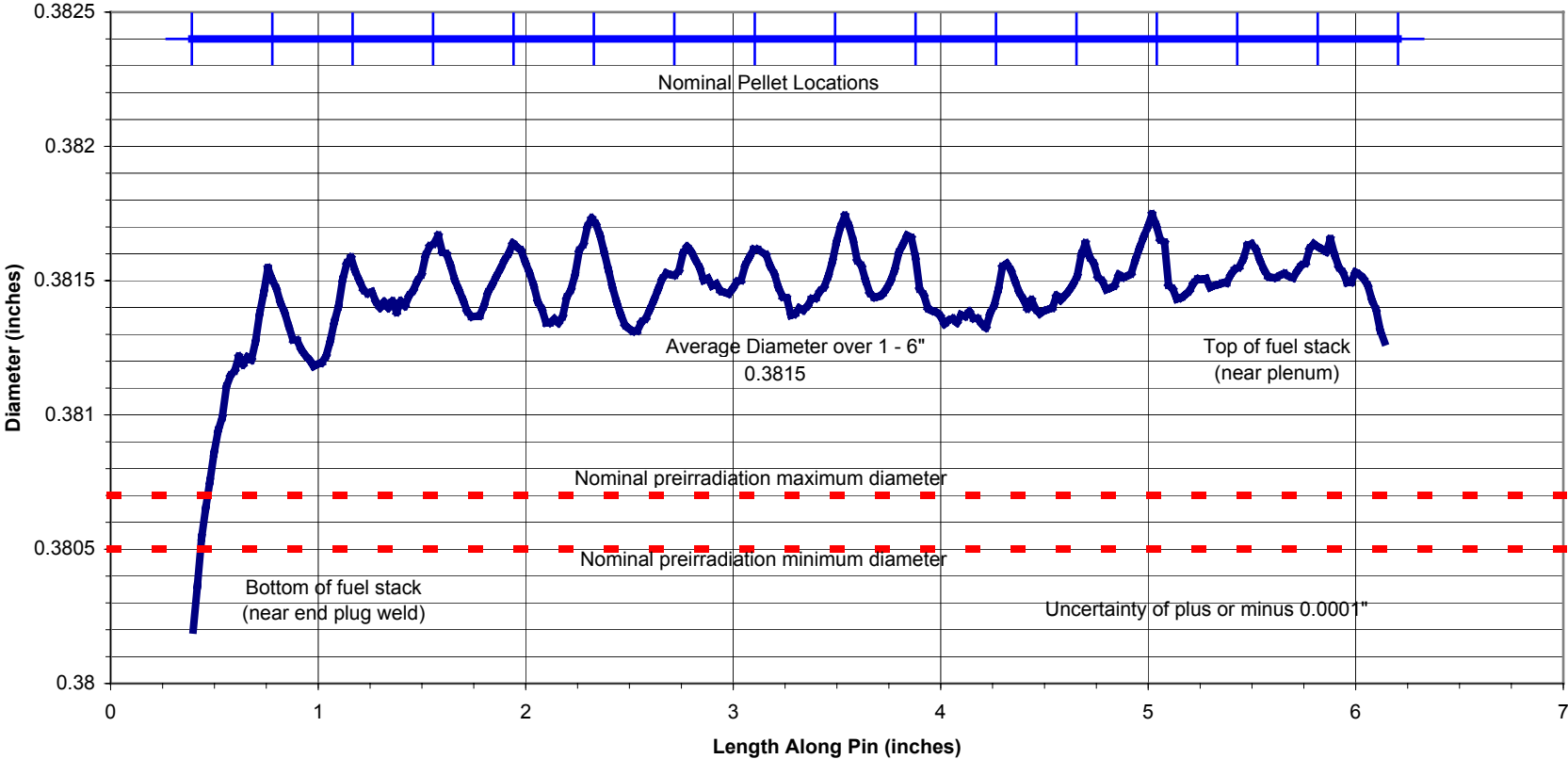
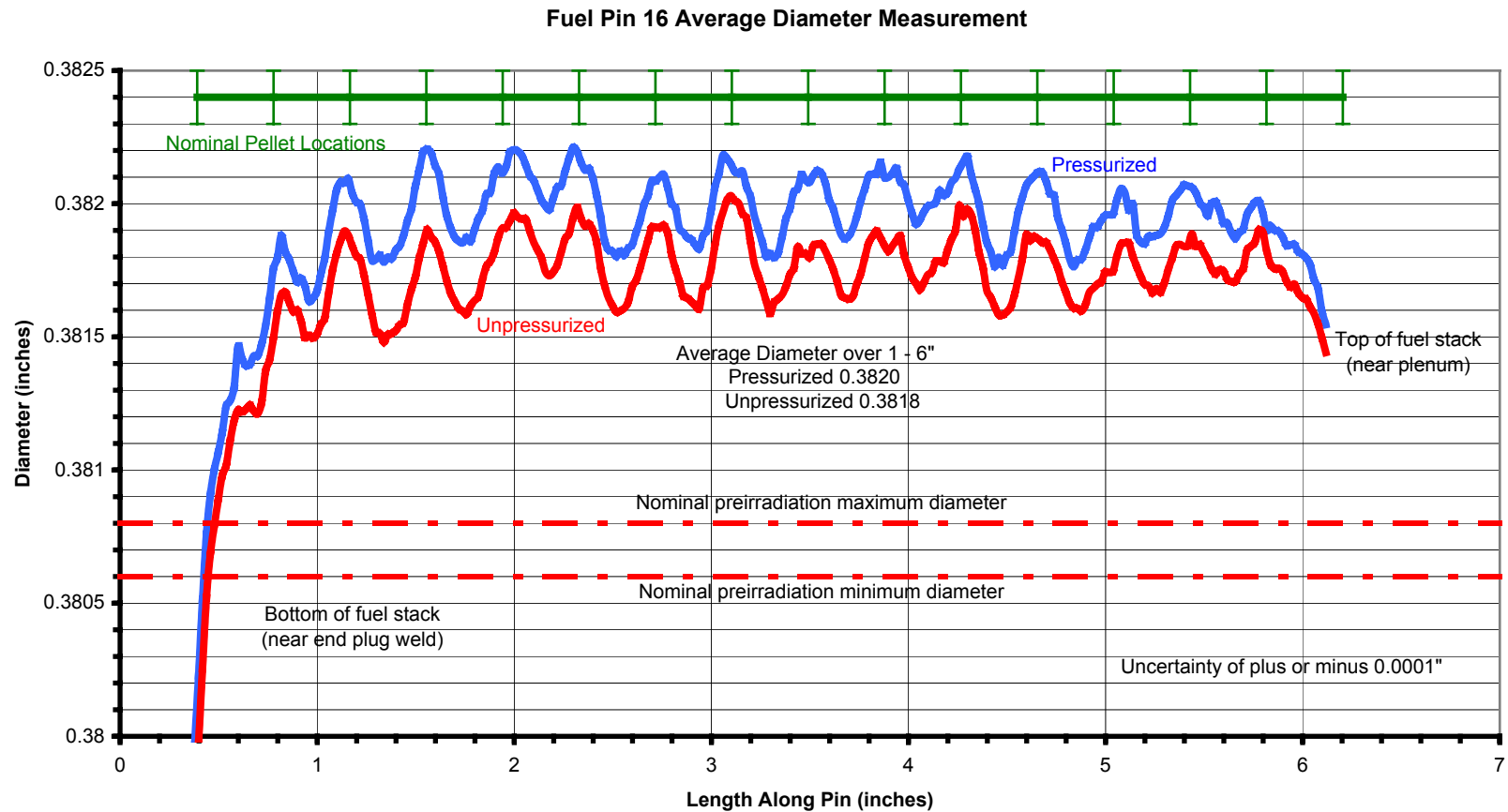
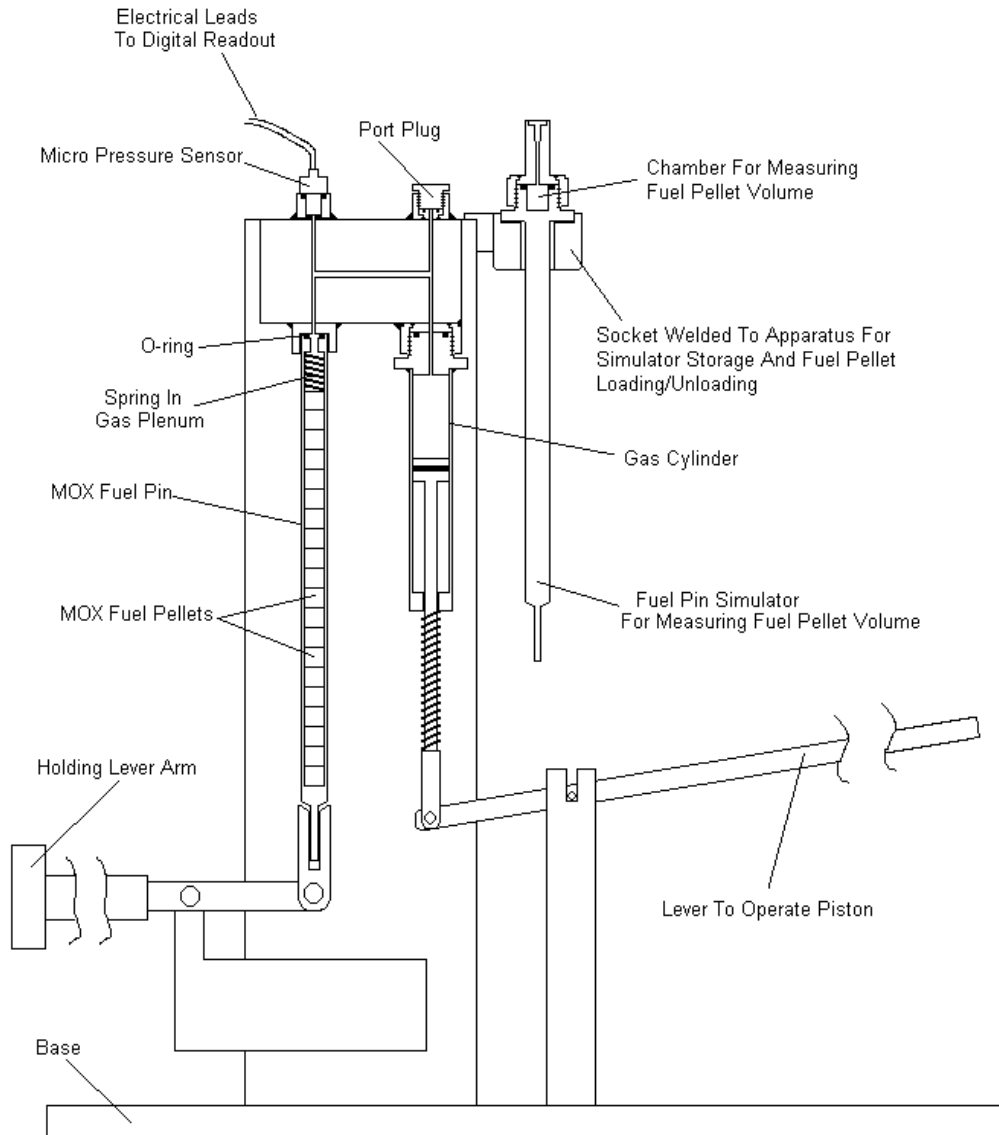


Figure 3.25. Graph of Fuel Pin 7 diametrical measurements.



**Figure 3.26. Graph of Fuel Pin 16 diametrical measurements. Both pressurized and unpressurized measurements are shown. (The unpressurized measurement had three small handling scratches at approximately 1.8, 2, and 3", which were removed from the graph for clarity)**



**Figure 3.27. Schematic of the Fuel Pin Volume Measuring Apparatus.**

## 4.0 CONCLUSIONS FROM QUICK LOOK PIE

Capsules 4 and 13 were visually and dimensionally examined. No signs of capsule damage or distortion were observed. Both capsules were gamma scanned and showed no signs of structural irregularities.

After sufficient time was allowed for  $^{131}\text{I}$  to decay to required levels, the capsules were drilled to sample their gas plenums, which were found to be at subatmospheric pressure and free of fission gas. Subsequently, the fuel pin free volume pressures and fission gas activities were measured at levels corresponding to fission gas releases higher than determined for this fuel in previous PIEs, but still lower than the European experience with MOX fuels with similar irradiation histories. The current fission gas release fractions are in the range from 0.062 to 0.068, based on the Kr-85 activity measurements.

The capsules were opened and the fuel pins removed. No signs of damage or distortion of the fuel pin clad were observed. In fact, the fuel pins slid out as indicated by the CARTS code calculations. Measurements of the fuel pin clad outer diameter showed the expected primary ridging and clad creep, which confirms the fuel behavior predictions.

Overall, this Quick Look suggests that Capsule 4 and Capsule 13 have handled their irradiations without incident. There are no indications of any mechanisms that might threaten the containment integrity of the sister capsules currently continuing their irradiation in the ATR.

When compared to the previous the PIEs, a hint of difference between the treated and untreated fuel seems to be developing in fission gas release behavior. Table 4.1 sums up the fission gas releases as determined by  $^{85}\text{Kr}$  activity measurements to date; note that the treated fuel appears to have a higher release at all burnups, but the gap has narrowed at 40 GWd/MT.

In this connection, it should be noted that the 40 GWd/MT withdrawals experienced the highest linear heat generation rates and hence the highest fuel temperatures of any MOX test irradiation capsules. Future PIE data will determine if this release differential holds for the 50 GWd/MT withdrawals, which will have a higher burnup, but attained under less challenging thermal conditions.

**Table 4.1 Fission Gas Release Results**

Burnup	Untreated Fuel		TIGR Treated Fuel	
	Number	Release	Number	Release
21 GWd/MT	Pin 5	1.4%	Pin 12	2.0%
30 GWd/MT	Pin 6	1.5%	Pin 13	2.3%
40 GWd/MT	Pin 7	6.2%	Pin 16	6.8%

## **5.0 ACKNOWLEDGMENTS**

The authors wish to thank Steve Childs, Lloyd Turner, Pat Howard, Tom Kenney, and Jeff Moody of the Irradiated Fuels Examination Laboratory Staff for their help with the MOX capsule PIE task.

## 6.0 REFERENCES

1. B.S. Cowell and S.A. Hodge, Fissile Materials Disposition Program Light-Water Reactor Mixed Oxide Fuel Irradiation Test Project Plan, ORNL/MD/LTR-78, Rev 2, May 2000.
2. R.N. Morris, C.A. Baldwin, C.M. Malone, N.H. Packan, *MOX Average Power Early PIE: 8 GWd/MT Quick Look*, ORNL/MD/LTR-163 Rev. 1, February 1999.
3. R.N. Morris, et. al., *MOX Average Power Early PIE: 8 GWd/MT Final Report*, ORNL/MD/LTR-172, November 1999.
4. R.N. Morris, et. al., *MOX Average Power Intermediate PIE: 21 GWd/MT Quick Look*, ORNL/MD/LTR-185, March 2000.
5. R.N. Morris, et. al., *MOX Average Power Intermediate PIE: 21 GWd/MT Final Report*, ORNL/MD/LTR-199, December 2000.
6. R.N. Morris, et. al., *MOX Average Power Test 30 GWd/MT PIE: Quick Look*, ORNL/MD/LTR-208, February 2001.
7. R.N. Morris, et. al., *MOX Average Power 30 GWd/MT PIE: Final Report*, ORNL/MD/LTR-212, Volume 1, November 2001.
8. R.N. Morris, *Post-Irradiation Examination Plan for ATR MOX Capsules Withdrawn at 30 GWd/MT and Higher*, ORNL/MD/LTR-195, September 2000.
9. C. Vitanza, E. Kolstad, and U. Graziani, *Fission Gas Release From UO<sub>2</sub> Pellet Fuel at High Burn-up*, ANS Topical Meeting on Light Water Reactor Fuel Performance, Portland, Oregon, 29 April–3 May, 1979.
10. S. A. Hodge, *Fission Gas Release and Pellet Swelling Within the High-Power Mixed-Oxide Irradiation Test Assembly*, ORNL/MD/LTR-128, Rev 1, November 1998.
11. W. K. Terry, *As-Run Radiological Characterization of MOX Fuel Capsules Removed From the ATR After Cycle 127A — WKT-03-02*, March 28, 2002.
12. L. Noirot, Ph. Garcia, and C. Struzik, *A Mechanistic Fission Gas Behaviour Model for UO<sub>2</sub> and MOX Fuels*, Fission Gas Behaviour in Water Reactor Fuels, Seminar Proceedings, Caderache, France, 26–29 September, 2000.
13. S. A. Hodge, L. J. Ott, F. P. Griffin, and C. R. Luttrell, *Implications of the PIE Results for the 30-GWd/MT-Withdrawal MOX Capsules*, ORNL/MD/LTR-212, Volume 2, Rev. 1, February 2002.

14. R.N. Morris, C.A. Baldwin, C.M. Malone, *MOX Fission Gas Pressure Measuring Apparatus*, ORNL/MD/LTR-176, January 2000.
15. R.N. Morris, C.A. Baldwin, *MOX Fuel Pin Measuring Apparatus*, ORNL/MD/LTR-209, March 2001.
16. R.N. Morris, D.W. Heatherly, *MOX Fuel Pin Volume Measuring Apparatus*, ORNL/MD/LTR-232, September 2002.

## 7.0 DISTRIBUTION

1. P.T. Rhoads, U.S. Department of Energy, MD-3, 1000 Independence Avenue SW, Forrestal Building 6G-050, Washington DC 20585
- 2-6. R.C. Pedersen, Idaho National Engineering and Environmental Laboratory, EROB, 2525 Fremont Avenue, Idaho Falls, ID 83415-3419
7. P. Kasik, MPR Associates Inc., 320 King Street, Alexandria, VA 22314-3238
8. C.A. Baldwin
9. B.S. Cowell
- 10-14. S.A. Hodge
15. D.W. Heatherly
20. L.L. Horton
21. M.W. Kennard, Stoller Nuclear Fuel, 485 Washington Avenue, Pleasantville, NY 10570
- 22-26. J.S. Tucker, Framatome Cogema Fuels, 3315 Old Forest Road, Lynchburg, Va 24506
- 27-31. R.N. Morris
- 32-36. N.H. Packan
37. L.J. Ott
38. D.J. Spellman
39. K.R. Thoms
40. G.L. Yoder, Jr.
41. S.J. Zinkle
42. ORNL Laboratory Records (RC)